Dear Dr. Qiang Wang,

Thank you very much for sending us the reviews of our revised manuscript.

The reviewer is satisfied with your revision, but it is suggested that you need to proofread the English writting, especially for the parts added during the last revision. Although you can have further chance to proofread your manuscript after it is accepted, in this case, I would suggest you to do it first before I accept your paper. A few examples provided by the reviewer are given below.

We carefully checked and improved the English writing in not only the parts added in the last revision but also the other parts as much as possible. We also fixed the several typos. Please see the details in the revised manuscript with the track changes. Our modifications do not change any contents in our paper.

Some minor issues/typos from my quick checks.

Line 79-80, negative sign "-" should be "~" or just use "approximately".
We deleted the negative sign.

Line 187, "the subtropical gyres……" changed to "the improvement in the subtropical gyres of the Atlantic and Indian Oceans is limited".
We corrected it.

Line 371, should add "has" before "a deeper".
We corrected it.

Line 373, remove "frequently" and add "all the time" after Kyushu.
We corrected the sentence: "the simulated Kuroshio in OFES2 is frequently makes an unrealistic excursion away from Kyushu.".

Line 376, change "makes significant" to "contribute mainly to the".
We corrected it.

Line 378, add well before "simulated".
We corrected it.

A global eddying hindcast ocean simulation with OFES2

Hideharu Sasaki[1], Shinichiro Kida[2,1], Ryo Furue[1], Hidenori Aiki[3,1], Nobumasa Komori[1], Yukio Masumoto[4,1], Toru Miyama[1], Masami Nonaka[1], Yoshikazu Sasai[5], Bunmei Taguchi[6,1]

[1]Application Laboratory, Japan Agency for Marine-Earth Science and Technology, Yokohama, Japan
5 [2]Research Institute for Applied Mechanics, Kyushu University, Kasuga, Japan
[3]Institute for Space-Earth Environmental Research, Nagoya University, Nagoya, Japan
[4]Graduate School of Science, The University of Tokyo, Tokyo, Japan
[5]Research Institute for Global Change, Japan Agency for Marine-Earth Science and Technology, Yokosuka, Japan
[6]Faculty of Sustainable Design, University of Toyama, Toyama, Japan
10

Correspondence to: Hideharu Sasaki (sasaki@jamstec.co.jp)

Abstract. A quasi-global eddying ocean hindcast simulation using a new version of our model called "OFES2" (Ocean General Circulation Model for the Earth Simulator version 2) was conducted to overcome several issues with unrealistic properties in its previous version "OFES". This paper describes the model and the simulated oceanic fields in OFES2 compared with OFES

15 and also observed data. OFES2 includes ~~A~~ a sea-ice model and a tidal mixing scheme~~, were implemented in OFES2, which was~~ is forced by a newly created surface atmospheric dataset called JRA55-do and simulated the oceanic fields from 1958 to 2016. We found several improvements in OFES2 over OFES: smaller biases in the global sea surface temperature and sea surface salinity and the water mass properties in the Indonesian and Arabian Seas. The time series of the Niño3.4 and Indian Ocean Dipole (IOD) indexes are somewhat better in OFES2 than in OFES. Unlike the previous version, OFES2 reproduces

20 more realistic anomalous low sea surface temperatures during a positive IOD event. One possible cause for these improvements in El Niño and IOD events is the replacement of the atmospheric dataset. On the other hand, several issues remained unrealistic, such as the pathways of the Kuroshio and Gulf Stream and the unrealistic spreading of salty Mediterranean overflow. Given the worldwide use of the previous version and the improvements presented here on it, the output from OFES2 will be useful in studying various oceanic phenomena with broad spatiotemporal scales.

25 ## 1 Introduction

The global ocean includes phenomena with various spatial scales. Basin-scale circulations occur over thousands of kilometers, while oceanic fronts, western boundary currents, and the Antarctic Circumpolar Current (ACC) have widths of approximately or less than 100 km. Mesoscale eddies, ubiquitous around these currents and in the ocean interior, have a spatial scale of a few tens of kilometers in the ~~sub-Arctic~~subarctic ocean to a few hundred kilometers in the subtropics (Chelton et al., 1998). The

30 location and strength of oceanic fronts, currents, and mesoscale eddies also change over time (e.g., Sasaki and Schneider, 2011; Qiu and Chen, 2010; Zhai et al., 2008).

Observations are crucial for understanding the ocean, but their data coverage and resolution are limited. Since the 2000s, gridded hydrographic products based on Argo float observations (e.g., Roemmich et al., 2009; Hosoda et al., 2008) have been able to capture global ocean properties at a resolution of approximately 300 km. However, such a spatial resolution is not adequate to observe resolve narrow currents, mesoscale eddies, and or frontal structures. Satellite observations can provide high-resolution data of the sea surface height (SSH) and temperature (SST), etc., but are limited to surface measurements. Global eddying simulations, therefore, have become a useful and convenient tool for understanding the ocean. Computational power has increased exponentially, and over past decades, several research groups have been conducting global eddying ocean simulations at horizontal resolutions of approximately 10 km using the Parallel Ocean Program (POP, Maltrud and McClean, 2005), the Hybrid Coordinate Ocean Model (HYCOM, Chassignet et al., 2006), the Max Planck Institute ocean model (MPIOM, Jungclaus et al., 2013), and the Ocean General Circulation Model (OGCM) for the Earth Simulator (OFES, Masumoto et al., 2004). The realistic long-term hindcast global eddying ocean simulation outputs from OFES have been widely used in the community (http://www.jamstec.go.jp/res/ress/sasaki/ofes_publication.html).

The outputs from global eddying ocean simulations have provided unprecedented information about oceanic phenomena on wide spatiotemporal scales in areas where observational data are limited. These simulations create a significant amount of data, which are very informative because the data exhibit oceanic phenomena from around the globe with the scales from mesoscales to large basin scales and their variations from intraseasonal to decadal timescales. Sharing simulation outputs among the community is crucial, and such use of OFES (Sasaki et al., 2008) has led to research achievements in various topics (see details in Masumoto 2010), such as in oceanic phenomena from intraseasonal (e.g., Hu et al. 2018) to decadal variations (e.g., Taguchi et al. 2017) and mesoscale eddies (e.g., Aoki et al. 2016). However, numerical models are not perfect. Model deficiencies and biases exist, and the usage of simulation outputs in the community has led to findings of where these limitations exist and their possible causes. One of the major problems of OFES seems to be its surface wind stress fieldsfield. Kutsuwada et al. (2019) showed that the thermocline depth in the subtropical northwestern Pacific was too shallow due to unrealistic wind stress. The second problem Another problem is the lack of tidally induced vertical mixing. Masumoto et al. (2008) found unrealistic water properties within the Indonesian seas, where tidally induced vertical mixing is considered significant (Ffield and Gordon, 1996). The third problem Another problem is the lack of sea ice. Therefore, because of which, the sea surface salinity in OFES was strongly restored to monthly climatological observations.

This paper highlights how an updated OFES improved the hindcast simulation outputs from OFES. This The updated model was forced by surface forcing based on 3-hourly atmospheric reanalysis data at a finer horizontal resolution. A tidal mixing scheme and a sea-ice model were added, and we call the standard hindcast simulation using this new version OFES2 (Fig. 1). Section 2 describes OFES2, and Section 3 examines its simulated mean oceanic fields, and Section 4 examines the time variability based on climate indexes of El Niño and the Indian Ocean Dipole Mode (IOD). We will further examine the IOD events and highlight the simulated SST distribution around the eastern pole of the IOD. A summary and discussion are provided in Section 5.

2 Descriptions of OFES2 compared with OFES

OFES2 is an update of a quasi-global eddying hindcast simulation: OFES (Sasaki et al., 2008). It is based on Modular Ocean Model (MOM) version 3 (Pacanowski and Griffies, 1999) and utilizes the latitude and longitude grid system. The horizontal resolution of 0.1° remains the same as that in OFES, but the model setup and parameterization are altered~~added~~ to reduce the model biases that exist in OFES. The model configuration of OFES2 will be described first, and the differences from OFES will be described next.

The domain extends from 76° S to 76° N without polar regions. The horizontal resolution is 0.1°, and the number of vertical levels is 105 with a maximum depth of 7,500 m. The thickness of each layer within the upper 100 m is 5 m. The thickness gradually increases and 55 levels exist within the upper 500 m. We constructed the bottom topography with partial bottom cells (Adcroft et al., 1997) using the bathymetry dataset ETOPO1 (Amante and Eakins, 2009). Although the model domain does not include the polar regions, a sea-ice model (Komori et al., 2005) was internally implemented into OFES2 to simulate the Antarctic ~~Sea~~ and ~~the~~ Subarctic oceans~~seas~~, including the Sea of Okhotsk, more realistically. The sea-ice model employs two-category, zero-layer thermodynamics (Hibler 1979) and elastic-viscous-plastic rheology (Hunke and Dukowicz, 2002).

A biharmonic operator is used for horizontal mixing to suppress computational noise with a viscosity of -27×10^9 m^4 s^{-1} and a diffusivity of -9×10^9 m^4 s^{-1}. The drag coefficient is 2.5×10^{-3} (non-dimensional) for linear bottom drag. For vertical mixing, we added diffusivities from the tidal mixing scheme developed by Jayne and St. Laurent (2001) and St. Laurent et al. (2002) to those estimated from the mixed layer vertical mixing scheme of a statistical closure model (Noh and Kim, 1999). In the tidal mixing scheme, the three-dimensional diffusivities are estimated from the energy flux at the ocean bottom and the local buoyancy frequency with the parameters of dissipation efficiency, mixing efficiency, and vertical scale. These parameters are the same as those used by St. Laurent et al. (2002). We used ~~a~~ constant barotropic tidal currents of K1 and M2 as the largest diurnal and semidiurnal tidal components in the FES2012 finite-element tide model (Carrère et al., 2012) and the bottom topographic slopes instead of roughness to estimate the energy flux at the ocean bottom (Tanaka et al., 2007). The simulated vertical diffusivities are large over rough bottom topographies and in areas with large tidal motions (Fig. 2a). The diffusivities exponentially decay in ~~an~~the upward direction (e.g., along 10° N in Fig. 2b). ~~These are similar to the simulated~~ The distributions of vertical diffusivities of Figs. 2a and 2b are similar to ~~Figs. 1 and 2 in the study by~~ St. Laurent et al.'s (2002; see their Figs. 1 and 2). The diffusivities do not change much over time because the tidal flow used to estimate the energy flux is assumed to be constant, and therefore, the diffusivities change in time only through changes in the local stratification.

We used the 3-hourly atmospheric surface dataset JRA55-do ver.08 (Tsujino et al., 2018) to estimate surface fluxes in OFES2. This dataset is based on the JRA55 atmospheric reanalysis at a horizontal resolution of approximately 55 km (Kobayashi et al., 2015). Momentum and heat fluxes are calculated with the bulk formulas proposed by Large and Yeager (2004). Note that we used the relative wind speed considering the surface current to estimate the surface momentum flux. We also included the effects of river runoff at river mouths as additional freshwater flux using a monthly mean climatological river runoff dataset from Coordinated Ocean-Ice Reference Experiments (CORE) version 2 (Large and Yeager, 2004). The sea

surface salinity (SSS) is restored to monthly climatological values of the WOA13 v2 observations (Zweng et al., 2013) with a 15-day timescale to avoid unrealistic salinity fields.

100   Since the polar regions are not simulated, the temperature and salinity are restored at all depths to the monthly climatological values from the same WOA13 v2 observations (Locarnini et al., 2013; Zweng et al., 2013) within a distance of 3° from the northern and southern boundaries of the model domain. The restoring time-scale linearly increases from 1 day at the boundary to infinity at the inner end of the restoring band. Additionally, the temperature and salinity near the straits of Gibraltar, Hormuz, and Bab el-Mandeb are restored to observations at all depths since the horizontal resolution of the model is inadequate to

105 capture dynamics within these straits (Fig. 3). The strait of Gibraltar is where the Mediterranean Sea ~~Atlantic Ocean~~ connects to the Atlantic Ocean ~~Mediterranean Sea~~ and the straits of Hormuz and Bab el-Mandeb are where the Persian Gulf and the Red Sea are connected to the Indian Ocean, respectively.

OFES (Sasaki et al., 2008) after 50 years of spin-up integration under climatological forcing (Masumoto et al., 2004) ~~,~~ ~~which follows a 50-year climatological simulation,~~ has been integrated from 1950 to the present ~~(Masumoto et al., 2004)~~.

110 OFES2 was integrated from 1958 to 2016 and started with the temperature and salinity fields of OFES from January 1, 1958. Table 1 is the list of the updates for OFES2 compared to OFES. The maximum depth of OFES2 is increased to 7,500 m from 6,065 m. The surface fluxes are now based on 3-hourly data rather than daily data to capture the diurnal cycle. Momentum fluxes are based on a bulk formula using the relative wind speed rather than that estimated in the reanalysis. The distribution of momentum flux curl in OFES2 differs much ~~compared with~~from that in OFES (Fig. S1). The mixed layer mixing scheme

115 is updated by replacing the KPP scheme based on an empirical approach (Large et al., 1994) by a statistical closure model (Noh and Kim, 1999). A tidal mixing scheme and a sea-ice model are newly included. The ~~River~~ river runoff is also added as additional freshwater flux. SSS is restored with a 15-day time scale rather than a 6-day timescale for the topmost 5-m layer: a 150-day time scale and a 60-day time scale ~~with respect to 50 m depth respectively~~, respectively, for a 50-m mixed layer. The timescale was relaxed compared to OFES, where neither sea ice nor river runoff was used.

3 Mean oceanic fields

120

We next discuss improvements in the mean oceanic fields in OFES2 from OFES by comparing those to the observations. The mean temperature and salinity fields at a horizontal resolution of 0.25° averaged over 2005-2012 from the World Ocean Atlas 2013 version 2 (WOA13, Locarnini et al., 2013, Zweng et al., 2013) are used, which include a large number of Argo float observations. During this period, both OFES2 and OFES were well spun up. Satellite-observed SSH over 1993-2016 from

125 AVISO is used to examine the simulated oceanic circulations and SSH variations in both OFES2 and OFES. To see how the sea-ice model works in OFES2, the climatological data of sea-ice cover averaged over 2005-2012 from HadISST version 1 (Rayner et al., 2003) is compared with the data in OFES2.

4

3.1 Global oceanic fields

3.1.1 Sea surface temperature and salinity

130   Figures 4a and 4c show the 8-year mean SST and SSS biases averaged over 2005-2012 in OFES2 against WOA13. For SST (Fig. 4a), the bias is less than 1°C in most parts of the globe. Weak cold bias broadly spread over the subtropical Pacific and Indian Oceans and the Arctic Ocean and weak warm bias spread over the subarctic Pacific, the subarctic Atlantic, and the Southern Ocean. We also found prominent biases in several regions. Warm biases (> 1 °C) appear in the South Pacific (170°-130° W and 55° S) and to the north of the Kuroshio Extension (140°-170° E and 35°-

135   40° N). In the North Atlantic, along the Gulf Stream and the North Atlantic Current and in the Labrador and Norwegian Seas, several large warm and cold biases (magnitudes larger than 1°C) are present. One possible cause of these biases is the unrealistic current pathway of the Gulf Stream. The Gulf Stream in OFES2 does not turn to the north at approximately 40° W, which we will examine more in detail in the next section.

       The mean SSS biases in OFES2 (Fig. 4c) are smaller than 0.2 psu in most regions. This feature is partly due to the restoring

140   surface boundary condition, but several large biases (larger than 0.2 psu) exist sporadically. The salty bias (> 0.4 psu) in the North Atlantic (30° W and 50° N) likely comes from the unrealistic Gulf Stream pathway, similar to the SST bias mentioned above. The salty bias (> 0.4 psu) also appears to the north of South America and in the northern part of the Bay of Bengal. Each salty bias surrounds a fresh bias. One reason for these large salty biases is probably the underestimation of river runoff from the Amazon and Ganges-Brahmaputra Rivers, respectively. The impacts of

145   physical processes near the river mouth such as horizontal and vertical mixing, coastal circulation, and tidal mixing should also be included to mitigate the biases. In addition, there are large salty and fresh biases in the Chukchi Sea and large salty biases in the Nordic and Labrador Seas and along the coast of Greenland. These SSS biases are possibly attributed to unrealistic sea-ice distribution in the Chukchi Sea (Fig. 9g) and unrealistic circulations due to the artificial northern boundary.

150   Figures 4b and 4d show the 8-year mean SST and SSS biases averaged over 2005-2012 in OFES against WOA13. The SST biases are much smaller in OFES2 (Fig. 4a) than in OFES (Fig. 4b). Cold (warm) SST biases with large amplitudes appear in the equatorial and subtropical regions (high-latitude regions) in both hemispheres in OFES. The centers of the cold biases (< −1°C) zonally spread along 15° N and 15° S in the Pacific Ocean and the northwestern and southeastern Indian Ocean. Patches of warm biases (> 1°C) exist in the Antarctic Ocean to the south of the ACC.

155   Prominent warm biases (> 1°C) appear in the northwestern Pacific, the Sea of Okhotsk, and along the west coasts of South America and Southern Africa. The prominent warm biases along the west coasts in OFES are presumably associated with unrealistic coastal currents and upwelling, which are driven by unrealistic wind stresses near the coasts in the NCEP reanalysis (Fig. S1). The reductions of these biases in OFES2 are likely a result of using the bulk formula (Large and Yeager, 2004) and the atmospheric surface data (JRA55-do) optimized to drive OGCMs (Tsujino et al., 2018). Additionally, the

160 implementation of a sea-ice model in OFES2 may contribute to the ~~decreases in~~reduction of the warm biases in the Arctic Ocean and the Sea of Okhotsk.

The mean SSS biases in OFES2 (Fig. 4c) are also much reduced compared to those in OFES (Fig. 4d), especially in the tropical and subtropical regions. These bias reductions are also likely due to the bulk formula and atmospheric data used in OFES2. We notice that the global distribution of the biases in OFES (Fig. 4d), prominent in the Arctic Ocean is quite similar

165 to the difference between WOA98 (Conkright et al., 1998) and WOA13 averaged over 2005-2012 (Fig. 4f). This similarity suggests that the SSS fields in OFES are too much restored to WOA98. In contrast, the global distribution of the SSS biases in OFES2 (Fig. 4c) does not resemble the difference between long-term mean WOA13 and WOA13 over 2005-2012 (Fig. 4e). The weak restoring in OFES2 does not greatly constrain the simulated SSS. Therefore, the SSS bias in OFES2 (Fig. 4c) comes from something other than the restoring such as the unrealistic path-ways of Kuroshio and Gulf Stream and the unrealistic sea-

170 ice distribution in the Chukchi Sea as mentioned above.

3.1.2 Sea surface height and its variability

Figure 5 shows the average and standard deviation of the sea surface height (SSH) over 1993-2016 in OFES2, OFES, and AVISO. The large-scale distribution of the mean SSH~~s~~ in OFES2 (Fig. 5a) agrees well with that in AVISO (Fig. 5c), suggesting that OFES2 reproduces the global ocean circulations well. The SSH variability (Fig. 5d) is large around the Gulf Stream, the

175 Kuroshio, and the ACC, which also resembles that in AVISO (Fig. 5f). This large variability is mostly due to high activities of mesoscale eddies and shifts in frontal positions (e.g., Chelton et al., 2007).

However, there are regional differences in the mean SSH distribution and its standard deviation in OFES2 ~~compared to~~from those in AVISO. The mean SSH contours along the Gulf Stream extend ~~towards the northeast~~northeastward across the Atlantic in OFES2 (Fig. 5a), while a sharp northern turn is observed at approximately 40° W in AVISO (Fig. 5c). The SSH variability

180 is large along this simulated Gulf Stream (Fig. 5d). The zonal extension of the mean SSH contours along with the Azores Current at approximately 33° N in the northeastern Atlantic (Fig. 5c) and large SSH variability ~~accompanied by~~accompanying this current (Fig. 5f) are recognizable in AVISO but ~~do~~ not ~~appear~~ in OFES2 (Fig. 5a and Fig. 5d). For the Kuroshio in OFES2, the SSH variability is too large along the southern coast of Japan. This large variability is due to the unrealistic detachment of the Kuroshio from Kyushu. Around subtropical countercurrents in the North Pacific and the South Indian Ocean and in most

185 regions away from the strong currents, the SSH variability is slightly smaller in OFES2 than in AVISO. We discuss these issues in Section 5.

Compared to OFES (Fig. 5b), the mean SSH in OFES2 (Fig. 5a) shows improvements. In the northern and southern subtropical gyres of the Pacific, the SSH contours are oriented more in the north-south direction in OFES (Fig. 5b) than in OFES2 and AVISO (Figs. 5a and 5c). In contrast, the improvement in the subtropical gyres of the Atlantic and Indian Oceans

190 is limited~~the subtropical gyres of the Atlantic and Indian Oceans do not have this difference~~. One possible cause for this improvement in the SSH field in OFES2 is the replacement of atmospheric wind driving OFES by JRA55-do. The overall amplitude of SSH variability around strong currents such as the Gulf Stream, the Kuroshio, and the ACC ~~(Fig. 5d) in OFES2~~

is ~~comparable~~ similar to that of AVISO ~~observations~~ (Fig. 5f) in OFES2 (Fig. 5d)~~,~~ ~~which is reduced somewhat compared to~~whereas it is somewhat larger in OFES (Fig. 5e). The northwestward ~~extent with~~extension of high SSH variability ~~to the west of~~emanating from the southern tip of South Africa~~,~~ ~~that corresponds to~~which represents the propagation~~s~~ of Agulhas ~~r~~Rings~~, is improved in OFES2, which~~ is too distinct in OFES due to unrealistic~~ally~~ long-lived rings. This problem is cured in OFES2. These reductions of SSH ~~-~~variability ~~reductions~~ in OFES2 are possibly due to eddy killing effect in the estimation of surface momentum flux using ~~the~~relative wind (e.g.~~,~~ Renault et al. 2017, 2019a).

3.2 Impact of tidal mixing on water mass property

~~Tidal mixing is considered to mix the ocean~~Internal tides enhance vertical mixing, especially above rough-bottom topography. Previous studies have suggested that the Indonesian seas are regions where such mixing significantly impacts the water mass properties (e.g., Ffield and Gordon, 1996). Koch-Larrouy et al. (2007) demonstrated how the inclusion of ~~the~~a local tidal mixing scheme can improve the subsurface water mass in the Indonesian seas and the eastern Indian Ocean. As mentioned in the introduction, unrealistic water mass properties in the subsurface of Indonesian Seas were one of the major biases recognized in OFES (Masumoto et al., 2008), which ~~motivated us~~was one of the motivations to add ~~the~~a tidal mixing scheme in OFES2.

A comparison of subsurface salinity biases in the Indonesian seas shows significant improvement in OFES2 (Figs. 6a and 6d) from OFES (Figs. 6b and 6e). The saltier bias at a depth of 135 m is large (> 0.5 psu) in the northern Banda Sea in OFES but is greatly reduced in OFES2. To the south of the Sunda Islands, the saltier biases are prominent both at depths of 135 m (> 0.2 psu) and 325 m (> 0.5 psu) in OFES but are greatly reduced in OFES2. The remaining salty biases in OFES2 may be partially due to lack of nonlocal tidal mixing (e.g. Nagai et al., 2017), as discussed in Sasaki et al. (2018). This result supports the importance of tidal mixing on the water mass transformation in the Indonesian seas.

The Kuril Strait between the North Pacific and the Sea of Okhotsk is another location where previous studies (e.g., Nakamura et al., 2006) suggested the importance of tidal mixing on the water mass properties of the North Pacific Intermediate Water (NPIW). The vertical section of salinity along 165° E in WOA13 shows ~~that~~ this subsurface low-salinity water~~is accompanied by the NPIW~~, which ~~both OFES2 and~~ OFES ~~demonstrates~~reproduces well and OFES2 does a little better (Fig. S2). ~~although this water mass distribution is improved a little more in OFES2 than in OFES.~~ Thi~~s~~e result suggests that ~~the~~tidal mixing ~~scheme in OFES2~~does not affect the ~~water~~properties of NPIW much, which supports the results using an eddy-permitting model by Tanaka et al. (2010). The vertical diffusivity of 0.02 m^{2}s^{-1} ~~Nakamura et al. (2006) may have added too large vertical diffusivity~~used ~~(0.02 m^{2}s^{-1})~~ in the strait at all depths in ~~their~~an OGCM in Nakamura et al. (2006) was probably too large. ~~, which probably led to too strong impacts on the water properties.~~

3.3 Salty outflows from marginal seas

OFES could not accurately simulate high-salinity outflows from the Mediterranean Sea, the Persian Gulf, ~~and~~or the Red Sea to the open ocean. To represent the impact~~s~~ of these outflows in OFES2, we restored temperature and salinity near the straits

(Section 2). Proper representations of these outflows are considered important for simulating not only the subsurface but also

225 the surface properties (e.g., Jia et al., 2000; Prasad et al. 2001; Sofianos and Johns, 2002).

Vertical sections of salinity averaged over 2005-2012 (Fig. 7) exhibit the salty outflows at the subsurface in the Arabian Sea and the Atlantic Ocean. For the Arabian Sea, the basic influence of the outflow appears to be captured in OFES2. The longitudinal section of mean salinity crossing the mouth of the Red Sea shows that OFES2 (Fig. 7a) mostly reproduces the eastward extent of salty water (> 35.5 psu) from 46° E at approximately 700 m depth~~, observed~~ in WOA13 (Fig. 7c). This

230 feature ~~corresponds to~~represents the salty outflow from the Red Sea. The eastward extension (> 35.5 psu), however, reaches too far at 70° E, and its depth of 700 m is too stable over the basin compared to that in WOA13. OFES2 (Fig. 7d) also generally demonstrates the southward spreading of salty outflow from the Persian Gulf: salty water (> 35.5 psu) spreads southward from 25° N above 1000 m in WOA13 (Fig. ~~6f~~7f). However, the high salinity core (> 35.5 psu) at a depth of 800 m is slightly too distinct and deep in OFES2 (Fig. 7d).

235 ~~However~~In contrast, we found that OFES2 does not well reproduce the salty outflow from the Mediterranean Sea into the Atlantic Ocean ~~well by restoring~~even with the restoration of temperature and salinity near the Strait of Gibraltar. A zonal vertical section of salinity along 36° N in the eastern Atlantic Ocean in WOA13 (Fig. 7i) exhibits the westward extension of salty water (> 35.8 psu) to 25° W at approximately 1100 m depth and a thick layer with almost constant salinity of 35.7 psu over 500-1100 m depths to the west of 26° W. However, the westward exten~~tent~~sion of high salinity is ~~still~~ weak in OFES2

240 (Fig. 7g). This high salinity (> 36.0 psu) remains to the east of 9° W at depths over 1000-1500 m, where OFES2 restores salinity to the observation (Fig. 3). It is not clear w~~W~~hy the salty water does not spread westward much in OFES2 ~~is unclear~~, but this phenomenon is possibly ~~be~~ connected to the bias found in the mid-ocean surface circulation in the North Atlantic (Figs. 5a and 5c). Entrainment of surface water to the Mediterranean outflow near the Strait of Gibraltar is suggested as the mechanism driving the Azores Current (Jia et al. 2000; Kida et al., 2008) and ~~turning northward of~~the northward turn of the

245 Gulf Stream (Jia et al., 2000).

~~The implementation of restoring temperature and salinity conditions~~ The temperature and salinity restoration at the straits resulted in significant improvements in the Arabian Sea from OFES~~. without the setup.~~ OFES2 reproduces the salty outflow from the Red Sea well (Fig. 7a) but OFES does not: there is no salty water at the subsurface along 13° N in the Arabian Sea (Fig. 7b). OFES2 also greatly improved the salty outflow from the Persian Gulf (Fig. 7d) from OFES (Fig. 7e). The meridional

250 section along 65° E shows that the ~~salinity of subsurface~~ salty subsurface outflow ~~in OFES (Fig. 7e)~~ is much fresher by 0.3-0.5 psu in OFES (Fig. 7e) than ~~that~~ in WOA13 (Fig. 7f), and its depth of 1000 m is deeper than ~~that~~ in WOA13 (800 m). For the Mediterranean outflow, the improvement in OFES2 from OFES is marginal. Both OFES2 (Fig. 7g) and OFES (Fig. 7h) cannot reproduce the westward extent of the salty outflow from the Strait of Gibraltar found in WOA13 (Fig. 7i).

3.4 Subsurface field in the subtropical North Pacific

255 The subsurface water properties are sensitive to the wind stress product used. Kutsuwada et al. (2019) showed that wind stress products affect the simulated oceanic fields in an OGCM not only at the surface but also in the subsurface. In the subtropical

8

Pacific along 10° N, where the subsurface bias is large in OFES (Fig. 4 of Kutsuwada et al. 2019), they found that the use of QuikSCAT wind stress (Kutsuwada, 1998) in another version of OFES, called OFES QSCAT (Sasaki et al., 2006), improves the subsurface water properties compared to OFES, which ~~using~~ uses wind stress from NCEP reanalysis (Kalnay et al., 1996).

260   The vertical profile of the mean temperatures in the subtropical Western Pacific in OFES2 (red curve) mostly overlaps with that in WOA13 (black curve) (Fig. 8a). The maximum difference occurs at 280 m and is less than 1 °C. This region is characterized by subsurface salinity maximum (e.g., Nakano et al., 2005). Its depth agrees between OFES2 and WOA13 (Fig. 8b), and its peak salinity value differs a bit by 0.2 psu.

We found that the temperature and salinity biases ~~in OFES2 improved~~ significantly reduced in OFES2 from OFES. In the

265 thermocline between 50 m and 350 m depths, the temperature is much lower in OFES (Fig. 8a, blue curve) than in WOA13 (black curve). The maximum difference is approximately 6 °C at a depth of approximately 150 m. The depth of the salinity maximum is much shallower in OFES (approximately 100 m depth) than in WOA13 (approximately 140 m depth) (Fig. 8b). The maximum difference in salinity between OFES and WOA13 is large (~0.4 psu). These biases are very similar to those found by Kutsuwada et al. (2019) in their comparison between OFES QSCAT and OFES (their Fig. 5). As Kutsuwada et al.

270 (2019) suggested, these large biases in OFES possibly come from ~~the surface momentum flux~~wind stress. The wind stress curl ~~from NCEP driving~~used in OFES along 10° N (blue curve in Fig. 8c) is relatively strong~~ and fluctuates considerably in the longitudinal direction~~, which results in the anomalously shallow thermocline via too large Ekman upwelling. The wind stress curl in OFES2 (red curve in Fig. 8c) estimated by using 10-m wind in JRA55-do is comparable in amplitudes and variations to the satellite observations (red curve in Fig. 3c of Kutsuwada et al., 2019). The similarity between wind stress curl in OFES2

275 and the satellite observations comes from modifications of 10-m wind in JRA55-do using ~~the~~ satellite observations (Tsujino et al., 2018).

3.5 Sea-ice distribution in OFES2

We implemented a sea-ice model in OFES2, which is not present in OFES. The domain of OFES2 excludes a large~~,~~ central part of the Arctic Sea and the southern-most parts of the Ross Sea and the Weddell Sea. Figure 9 shows the distribution of

280 monthly climatological sea-ice cover in the polar regions averaged over 2005-2012 compared to the observations from HadISST. The sea-ice cover around Antarctica in March is realistic in OFES2 (Fig. 9a). The simulated sea ice covers most areas of the Weddell Sea, as found in HadISST (Fig. 9b). A small amount~~bit~~ of sea ice remains along the most coastline of East Antarctica (right side of the figure) in HadISST. ~~However, ,~~ whereas OFES2 misses the observed sea-ice cover near the coast from 90° E to 180° E. The sea-ice cover ~~distribution~~ greatly expands in September ~~expands greatly~~ compared to March

285 in HadISST (Fig. 9d), and OFES2 ~~exhibits~~ reproduces this~~its~~ sea-ice distribution~~s~~ very well (Fig. 9c). Off the coast of Victoria Land between 180° E and 150° E (lower side of the figure) and along the southern boundary of the model domain (76° S) in the Ross Sea (160° E-150° W), the sea-ice concentration ~~in OFES2~~ is somewhat lower in OFES2 than in HadISST.

In the Arctic region, t~~T~~he observed sea ice ~~in the Arctic region in March~~ covers the Chukchi Sea in March and seeps into the Bering Sea through the Bering Strait (Fig. 9f). OFES2 reproduces this feature~~the observations~~ well (Fig. 9e). However, the

9

290 simulated sea ice spreads too much southward into marginal seas: the Baltic Sea, the Gulf of Saint Lawrence, and the Sea of
Okhotsk. In September, unrealistic sea-ice cover spreads in the Chukchi Sea (Fig. 9g), which does not exist in HadISST (Fig.
9h). This ~~defect~~discrepancy is possibly due to the artificial northern boundary in OFES2, which blocks the ~~sea~~sea-ice outflow
~~(Kwok et al. 2004)~~through the Fram Strait (Kwok et al. 2004).

Observations show a multi-decadal decreasing trend in summer to fall sea-ice cover in the Arctic Region (compare Fig.S3h
295 with Fig.9h). ~~The observed sea ice in September in the Arctic region decreased much: relatively small extent of the sea ice in 2005-2012 (Fig. 9h) compared with that in 1980s (Fig. S3h).~~ However, OFES2 fails to ~~simulate the~~capture this trend probably
because of the limited domain, which does not cover most of the Arctic Sea. In the Antarctic region, no comparable trend
exists ~~the extent of sea ice appears not to change much~~ in either OFES2 ~~and~~or observations (Fig. 9a-d, Fig. S3a-d).

4 Interannual variations

300 ### 4.1 Niño3.4 and Indian Ocean Dipole Mode indexes

We examine the monthly time series of indexes for El Niño and IOD events to determine how well OFES2 reproduces these
variations over 1968-2016 (Fig. 10 and Table 2), excluding the initial ten years to avoid potential impacts of the initial
conditions.~~.~~ HadISST version 1 (Rayner et al., 2003) is used as the reference because it covers the whole analysis period. In
HadISST, however, the anomalous SST in the eastern pole during the IOD events, which is discussed in Section 4.2, appears
305 to be obscure.

The variation~~s~~ in the Niño3.4 index ~~is~~are very similar between OFES2 and HadISST (Fig. 10a). The correlation of ~~indexes~~
the index ~~between OFES2 and HadISST~~ is very high (0.963), and its RMS amplitude ~~of OFES2 (0.95 °C)~~ is slightly larger in
OFES2 (0.95 °C) than in ~~the observed value~~HadISST (0.89 °C). For IOD, the Dipole Mode Index (DMI) time series ~~in OFES2~~
is also similar ~~to that in~~between OFES2 and HadISST (Fig. 10b). The correlation ~~between~~of the DMI ~~of~~between OFES2 and
310 HadISST is high (0.714), but its RMS amplitude ~~in OFES2 (0.52 °C)~~ is considerably larger in OFES2 (0.52 °C) ~~than~~than in
HadISST (0.32 °C).

In OFES, the indexes of El Niño and IOD events are also similar to those in HadISST (see Table 2 for the correlations and
RMS amplitudes), with somewhat lower correlations than in OFES2. ~~One~~A possible cause for these high correlations in OFES2
is the replacement of atmospheric dataset by JRA55-do to estimate surface fluxes because usually SST in the ocean models is
315 strongly constrained to the atmospheric data via the surface flux. The RMS amplitudes in OFES (0.93 °C for Niño3.4 index
and 0.38 °C for DMI) are comparable to those of HadISST. The reason why the DMI RMS amplitude is larger in OFES2
(0.52 °C) than in OFES or the HadISST (0.32 °C) is the variations of ~~SSTA~~SST anomaly (SSHA)~~variations~~ simulated in the
eastern pole of the IOD. The SSTA~~s in the eastern pole in OFES2 are~~is colder (warmer) ~~mostly~~in the positive (negative) IOD
years of 1982, 1983, 1994, 1997, and 2006 (1996, 1998, and 2010) in OFES2 than in OFES and HadISST (Fig. 10c). The
320 amplitude of SSTA variations ~~show that its amplitude in OFES2 (0.43 °C)~~ is much larger in OFES2 (0.43 °C) than in OFES
(0.33 °C) and HadISST (0.33 °C). On the other hand, OFES2 ~~exhibits~~reproduces well the time series of ~~observed~~SSTA in

the western pole (Fig. 10d), with ~~the correlation of the SSTA~~a correlation coefficient of 0.847 between OFES2 and HadISST ~~being 0.847. This value is higher than~~as compared with 0.751 ~~from~~ between OFES ~~and HadISST~~. In OFES, the ~~warm biases~~SSTA ~~increase~~rises greatly after 2005. The ~~RMS~~ amplitude of SSTA variations is similar ~~amplitudes~~ between ~~in~~ OFES2

325   (0.31 °C) and HadISST (0.33 °C), which ~~are~~is relatively small compared to ~~that in~~ OFES (0.41 °C). ~~Therefore~~In the next section, we will closely examine this SST distribution around the eastern pole in a ~~the~~typical positive and a typical negative IOD year~~s next~~.

4.2 Sea surface temperature around the eastern pole of the Indian Ocean Dipole

We examine a strong positive and a strong negative IOD event~~s of~~in 1997 and 2010, respectively, as typical cases. ~~The~~

330   ~~s~~Satellite observations captured a low SST (< 26 °C) area ~~in the nearshore area~~ to the southwest of Sumatra and Java during the positive event (Fig. 11c). This anomaly is due to the coastal upwelling induced by~~The~~ anomalous southeasterly wind ~~induces coastal upwelling, and therefore, the SST near the coast becomes low compared with the offshore SST~~. OFES2 (Fig. 11a) reproduces this observed anomalous cold SST along the coast well, although the SST near Java is too cold (< 22 °C). During the negative event, the satellite-observed SST was warm (~30 °C) to the west of Sumatra (Fig. 11g). OFES2 (Fig. 11e)

335   also ~~exhibit~~capture~~s~~s this ~~observed~~ warm SST well. This warming is presumably due to weak upwelling from ~~the~~ weak wind west of Sumatra (Fig. 11e). OFES2 reproduces ~~the~~ cold and warm SST anomalies well in the eastern pole ~~of these and~~also in other ~~(Fig. S4)~~IOD events (Fig. S4).

    ~~We used the DMI estimated from HadISST version 1 (Rayner et al. 2003) as the observational index because HadISST covers a long period: 1871 to the present. However,~~ In contrast, HadISST in Fig. 11d (Fig. 11h) ~~is incapable of capturing~~does

340   not capture the cold (warm) SST near the southwestern coast of Sumatra and Java in the selected typical positive (negative) IOD event. Therefore, the DMI amplitude from HadISST is likely to be ~~too small~~smaller than the reality. In contrast, OISST v2 (Reynolds 1988), covering ~~the~~ a relatively short period from 1981 to the present, ~~exhibits~~ reproduces well the anomalous SST near the coast both in the positive and negative IOD events (Fig. S5), which is similar to the satellite observations (Figs. 11c and 11g). The average amplitude of the DMI over 1981-2016 is 0.54 °C for OISST v2, which is comparable to 0.54 °C

345   for OFES2. These results suggest that OFES2 well reproduces ~~the anomalous~~ SST anomalies near the southwestern coast of Sumatra and Java during IOD events and exhibits both the variation~~s in~~ and ~~the~~amplitude~~s~~ of the DMI well.

    OFES (Fig. 11b) did not accurately reproduce the observed anomalous cold SST (Fig. 11c) near the Sumatra and Java during the mature positive IOD event in 1997. The SST in OFES remains unrealistically warm (> 26 °C) to the southwest of Sumatra and Java. We attribute this fault to the wind stress driving OFES. The strong southeasterly wind stress (thick arrows, > 0.05 N

350   m^{-2}) is located far offshore (Fig. 11b), which cannot induce coastal upwelling with realistic strength. On the other hand, the anomalous warm SST in the eastern pole during the negative IOD in 2010 is fairly realistic in OFES (Fig. 11f), although the SST in the entire region is somewhat colder than from the satellite observations (Fig. 11g). This cold SST bias seems consistent with the bias all over the Indian Ocean in the long-term mean in OFES (Fig. 4b). These features generally apply to other IOD

11

events (Fig. S4). The difference in the SST reproducibility in the eastern pole between the positive and negative events in
355   OFES probably comes from the asymmetric property of the IOD events (e.g., Hong et al., 2008).

5 Summary and discussion

This paper describes a new version of our OGCM, which we call OFES2. OFES2 improves the atmospheric forcing to include
the diurnal cycle and now includes a tidal mixing scheme and a sea-ice model. We have presented how well OFES2 simulates
the mean oceanic features and interannual variations such as El Niño and IOD events, which are generally improved compared
360   to OFES (Table 3).

OFES2 reproduces large-scale circulations ~~,~~ and global distributions of mesoscale eddy ~~activities~~activity, SST~~s~~, and SSS~~s~~
well with significant improvements found in the water mass properties in the subsurface in the subtropical Western Pacific
and the Arabian and Indonesian Seas over OFES. OFES2 also represents the large SSHA RMS accompanied by strong currents
well, such as the Gulf Stream and the Kuroshio, ~~which is~~where SSHA RMS tends to be ~~somewhat~~ too large in OFES. However,
365   the RMS values are slightly smaller in most regions in OFES2 than in ~~the~~ satellite observations. The surface momentum fluxes
in OFES2 are estimated with a bulk formula by using the surface wind relative to the simulated surface current. This method
weakens mesoscale eddies, as Zhai and Greatbatch (2007) and Renault et al. (2019a) suggested, which ~~possibly damps the~~
~~SSHA RMS a bit too much~~may be the reason for the underestimation of SSHA RMS in OFES2. ~~Considering~~Taking into
account ~~the~~ atmospheric response~~s~~ to ~~the~~ SST ~~distributions~~gradients, such as impacts on ~~vertical mixing in the atmospheric
370   boundary layer (e.g., Wallace et al., 1989) and pressure adjustment over ~~the~~ SST fronts (e.g., Lindzen and Nigam, 1987), in
OGCM may be ~~one of the~~a solution~~s~~ to overcome this issue. Renault et al. (2019b) also showed the imprints of surface currents
on surface atmospheric winds through surface momentum flux in ~~the~~ satellite observations and coupled model simulations.
Sensitivity ~~experiments~~ on the coupling coefficients (Renault et al. 2020) is an interesting subject of futures study.~~remain as
our near future work.~~
375   The variations of the climate indexes of Niño3.4 and DMI are also well simulated in OFES2. The correlations of the monthly
indexes between OFES2 and ~~the~~ observations are slightly higher than for OFES. During ~~a~~the typical positive IOD event,
anomalous southeasterly wind near the Sumatra and Java induces ~~anomalous~~ cold ~~SST anomalyfields~~SSTA via coastal
upwelling. OFES2 reproduces this anomalous SST distribution well during typical events, which is due to the realistic surface
winds of JRA55-do driving OFES2. Other various climate variations are yet to be examined. ~~In addition,~~As a preliminary
380   exploration, we looked at the Atlantic Multidecadal Oscillation (AMO, Enfield et al. 2001).~~ was examined, although the period
of OFES2 over 1958-2016 is rather short.~~ The monthly AMO index in OFES2 varies with the observation with a correlation
coefficient~~value~~ of 0.90, ~~which is~~ much higher than 0.54 for OFES (Fig. 12). ~~Other various climate variations are yet to be
examined.~~

There are several issues in OFES2 that remain unrealistic from OFES. For example, parts of the pathways of the Kuroshio
385   and Gulf Stream are unrealistic, which created ~~a~~ strong SST bias (Fig. 4a and 4b) and unrealistic SSHA RMS variability (Fig.

5d and 5e) around these currents. ~~OFES2~~ We use~~s~~ ~~the~~ wind velocity relative to the surface current to estimate the surface momentum fluxes and a deep maximum bottom depth~~a deeper maximum bottom depth~~ (7,500 m), as Tsujino et al. (2013) and Kurogi et al. (2016) did to solve these issues for the Kuroshio. Nevertheless, the simulated Kuroshio in OFES2 ~~is~~ frequently ~~has~~makes an unrealistic~~ally~~ ~~path detached detaching~~offshore excursion away from Kyushu. To simulate ~~the~~a realistic Gulf

390 Stream separation, the importance of the sub-grid parameterization (Schoonover et al. 2016), adequate topographic resolution (Schoonover et al. 2017), ageostrophic circulation, and ~~front~~ frontogenesis (McWilliams et al. 2019) were suggested. Chassignet and Xu (2017) also succeeded in simulating the separation in a simulation at a horizontal resolution of 1/50°~~°—~~. In OFES2, the unrealistic path~~way~~ of the Gulf Stream ~~makes significant~~contributes mainly to the biases in SST, SSS, and SSH. Sensitivity experiments similar to the previous studies are needed to overcome this problem in OFES2.

395 The Azores Current was also not well simulated even with a restoring condition to reproduce the impact of the salty Mediterranean outflow, which we anticipated ~~would establish~~ driv~~e~~ing the Azores Current as suggested by~~in~~ Jia et al. (2000). An interesting result is that the Azores Current and the outflow do exist in the 1960s, but the both abruptly start to decay in the 1970s and disappear after the 1980s (see Figs. S6 and S7 for details). We have not yet found the ~~cause of~~reason for this behavior.

400 The impacts of the Mediterranean outflow on ~~the~~ deep meridional overturning were also suggested by previous studies (e.g. Reid 1979, McCartney and Mauitzen 2001). The overturning circulation in the Atlantic Ocean in OFES2 (Fig. S8) appears realistic but more detailed ~~examinations~~ analysis ~~are needed~~would be necessary to ~~improve~~ assess the Atlantic circulations over~~in~~ the whole depths. The salty outflows into the Arabian Sea and the water mass properties in the Indonesian Seas are improved in OFES2 with the restoring of temperature and salinity near the straits and with the tidal mixing scheme, respectively.

405 ~~Obviously, t~~There are more issues to investigate water mass properties in other regions in the future.

Another issue in OFES2 is that the domain does not include the polar regions in the latitudes higher than 76°. The sea-ice distribution is unrealistic in the Arctic region (Fig. 9e and 9g), whose decreasing trend is not also simulated. One possible reason for these defects is the existence of the northern boundary in OFES2 as discussed in Section 3.5. On the one hand, the meridional overturning circulations in the globe and Atlantic Ocean (Fig. S8) seem reasonable as mentioned above. A century-

410 scale integration would be necessary to pursue this issue.

The ~~The l~~L~~l~~atest supercomputer systems ~~enable us to perform~~have made possible global eddying ocean simulations with much less computational cost than before. Sensitivity experiments are becoming more feasible. Sasaki et al. (2018) showed that the inclusion of a tidal mixing scheme can result in an enhancement in ITF transport due to the basin-scale SSH increase in the tropical Pacific Ocean. While the direct impact of tidal mixing is local, its impact appears to spread over a whole basin

415 via Rossby and Kelvin waves (Furue et al. 2015). Ensemble simulations are another way of utilizing computational power. Nonaka et al. (2016) conducted a 3-member ensemble simulation using OFES ~~,~~ and ~~they~~ suggested the existence of intrinsic variations in the midlatitude ocean currents. One future direction of global, multidecadal, eddying ocean simulation is to obtain a large ensemble.

13

Global or basin-scale simulations capable of resolving oceanic submesoscales with ~~a~~ finer horizontal resolution (e.g., Sasaki
et al. 2014, Qiu et al. 2018) are also being pursued. However, it is still difficult to ~~execute~~ carry out these simulations over
many decades due to the huge demands on computational resources and storage. The causes behind model biases in eddying
simulations are still unresolved, and we still have much to learn from these simulations. Our improved hindcast simulation
will be useful for exploring oceanic processes and for Lagrangian analyses of water mass properties (e.g., Kida et al., 2019).
We hope that OFES2 will serve as a valuable tool for studying various oceanic features with wide spatiotemporal scales from
mesoscale to large-scale circulation and from intraseasonal to decadal timescales.

Author contribution

H. Sasaki and S. Kida implemented a tidal scheme and N. Komori implemented a sea-ice model into OFES2. H. Sasaki, S.
Kida, and R. Furue wrote the manuscript. H. Aiki, Y. Masumoto, T. Miyama, M. Nonaka, Y. Sasai, and B.Taguchi contributed
model configurations and writing the manuscript.

Code and data availability

OFES and OFES2 are based on MOM3, which is available through https://github.com/mom-ocean/MOM3. The code has been
modified for large-scale high performance simulation and implementations of sea-ice model and tidal mixing scheme. The
modification is copyrighted by Japan Agency for Marine-Earth Science and Technology (JAMSTEC). The modified code,
scripts, and input data to run OFES and OFES2 are available under a copyright agreement. ~~Monthly fields from OFES2 become
available in the immediate future.~~ Monthly fields from OFES2 and OFES can be downloaded from
https://doi.org/10.17596/0002029.

We thank Hiroyuki Tsujino for providing us with the earlier version of the JRA55-do dataset before the official release of
the latest version (https://esgf-node.llnl.gov/search/input4mips/). The river runoff dataset from CORE version 2 was
downloaded from https://data1.gfdl.noaa.gov/nomads/forms/core/COREv2.html. The ocean bathymetry from ETOPO1
(http://doi.org/10.7289/V5C8276M) was used. WOA13 and WOA98 are available at https://www.nodc.noaa.gov/OC5/woa13/
and ~~–~~https://www.esrl.noaa.gov/psd/data/gridded/data.nodc.woa98.html, respectively. The HadISST was downloaded from
https://www.metoffice.gov.uk/hadobs/hadisst/. AMSR-E SST version 7 and AVHRR SST version 4.1 were used through
APDRC (http://apdrc.soest.hawaii.edu/~~index.php~~). The AMSR data are produced by Remote Sensing Systems and were
sponsored by the NASA AMSR-E Science Team and the NASA Earth Science MEaSUREs Program. AVHRR Pathfinder
SST~~s were~~ was made by GHRSST and the US National Oceanographic Data Center. The AVISO SSH data and FES2012 tidal
current speeds were downloaded through Aviso (ftp://ftp.access.aviso.altimetry.fr). The monthly Niño3.4 index, DMI, and
AMO~~s~~ ~~for HadISST~~ were downloaded from http://www.cpc.ncep.noaa.gov/data/indices/,

14

http://www.jamstec.go.jp/aplinfo/sintexf/iod/___dipole_mode_index.html, and https://psl.noaa.gov/data/timeseries/AMO, respectively.

References

Adcroft, A., Hill, C., and Marshall, J.: Representation of topography by shaved cells in a height coordinate ocean model, Mon. Wea. Rev., 125(9), 2293–2315, doi:10.1175/1520-0493(1997)125<2293:ROTBSC>2.0.CO;2, 1997.

Amante, C. and Eakins, B. W.: ETOPO1 1 arc-minute global relief model: procedures, data sources and analysis. NOAA Technical Memorandum NESDIS NGDC-24, 19 pp, March 2009. http://www.ngdc.noaa.gov/mgg/global/global.html, 2009.

Aoki, K., Kubokawa, A., Furue, R. and Sasaki, H.: Influence of eddy momentum fluxes on the mean flow of the Kuroshio Extension in a 1/10° Ocean General Circulation Model, J. Phys. Oceanogr., 46 (9), 2769–2784, doi:10.1175/JPO-D-16-0021.1, 2016.

Carrère, L., Lyard, F., Cancet, M., Guillot, A., and Roblou, L.: FES 2012: a new global tidal model taking advantage of nearly 20 years of altimetry. In: Proceedings of meeting "20 Years of Altimetry", Venice, 2012.

Chassignet, E. P., Hurlburt, H. E., Smedstad, O. M., Halliwell, G. R., Wallcraft, A. J., Metzger, E. J., Blanton B. O., Lozano, C., Rao, D. B., Hogan, P. J., and Srinivasan, A.: Generalized vertical coordinates for eddy-resolving global and coastal ocean forecasts, Oceanography, 19(1), 118–129. Doi:10.5670/oceanog.2006.95, 2006.

Chassignet, E.P. and Xu, X.: Impact of horizontal resolution (1/12° to 1/50°) on Gulf Stream separation, penetration, and variability. J. Phys. Oceanogr., 47, 1999–2021, doi:10.1175/JPO-D-17-0031.1, 2017.

Casey, K. S., Brandon, T. B., Cornillon, P., and Evans, R.: The past, present and future of the AVHRR Pathfinder SST program, in Oceanography from Space, edited by: Barale, V., Gower, J. F. R., and Alberotanza, L., Springer, doi:10.1007/978-90-481-8681-5_16, 2010.

Chelton, D. B., deSzoeke, R. A., Schlax, M. G., El Naggar, K., and Siwertz, N.: Geographical variability of the first baroclinic Rossby radius of deformation, J. Phys. Oceanogr., 28(3), 433–460. Doi:10.1175/1520-0485(1998)028<0433:GVOTFB>2.0.CO;2, 1998.

480 Chelton, D. B., Schlax, M. G., Samelson, R. M., and de Szoeke, R. A.: Global observations of large oceanic eddies, Geophys. Res. Lett., 34, L15606, doi:10.1029/2007GL030812, 2007.

Conkright, M.E., Levitus, S. O'Brien, T., Boyer, T. P., Stephens, C., Johnson, D., O. Baranova, Antonov, A., Gelfeld, R., Rochester, J., and Forgy, C.: World Ocean Database 1998 Documentation and Quality Control, National Oceanographic Data Center, Silver Spring, MD, 1998.

485 Enfield, D.B., Mestas-Nunez, A.M., and Trimble, P.J.: The Atlantic Multidecadal Oscillation and its relationship to rainfall and river flows in the continental U.S., Geophys. Res. Lett., 28 (10), 2077–2080, doi: 10.1029/2000GL012745, 2001.

Ffield, A., and Gordon, A. L.: Tidal mixing signatures in the Indonesian Seas, J. Phys. Oceanogr., 26(9), 1924–1937, doi:10.1175/1520-0485(1996)026<1924:TMSITI>2.0.CO;2, 1996.

Furue, R., Jia, Y., McCreary, J. P., Schneider, N., Richards, K. J., Müller, P., Cornuelle, B. D., Avellaneda, N. M., Stammer,
490 D., Liu, C., and Köhld, A.: Impacts of regional mixing on the temperature structure of the equatorial Pacific Ocean. Part 1: Vertically uniform vertical diffusion, Ocean Modell., 91, 91–111, doi.org:10.1016/j.ocemod.2014.10.002, 2015.

Hibler III, W. D.: A dynamic thermodynamic sea ice model, J. Phys. Oceanogr., 9(4), 815–846, doi:10.1175/1520-0485(1979)009<0815:ADTSIM>2.0.CO;2, 1979.

Hong, C., Li, T., LinHo, and Kug, J.: Asymmetry of the Indian Ocean Dipole. Part I: Observational analysis, J. Clim., 21(18),
495 4834–4848, doi:10.1175/2008JCLI2222.1, 2008.

Hosoda, S., Ohira, T., and Nakamura, T.: A monthly mean dataset of global oceanic temperature and salinity derived from Argo float observations. JAMSTEC Report of Research and Development, 8, 47–59, doi:10.5918/jamstecr.8.47, 2008.

Hu, S., Sprintall, J., Guan, C., Sun, B., Wang, F., Yang, G., Jia, F., Wang, J., Hu, D., and Chai, F.: Spatiotemporal features of intraseasonal oceanic variability in the Philippine Sea from mooring observations and numerical simulations, J. Geophys.
500 Res.: Oceans, 123 (7), 4874– 4887, doi:10.1029/2017JC013653, 2018.

Hunke, E. C., and Dukowicz, J. K.: The elastic–viscous–plastic sea ice dynamics model in general orthogonal curvilinear coordinates on a sphere—Incorporation of metric terms, Mon. Wea. Rev., 130(7), 1848–1865. doi:10.1175/1520-0493(2002)130<1848:TEVPSI>2.0.CO;2, 2002.

Jayne, S. R., and St. Laurent, L. C.: Parameterizing tidal dissipation over rough topography, Geophys. Res. Lett., 28(5), 811–
505 814, doi:10.1029/2000GL012044, 2001.

Jia, Y. (2000). Formation of an Azores Current due to Mediterranean overflow in a modeling study of the North Atlantic, J. Phys. Oceanogr., 30(9), 2342–2358, doi:10.1175/1520-0485(2000)030<2342:FOAACD>2.0.CO;2, 2000.

Jungclaus, J. H., Fischer, N., Haak, H., Lohmann, K., Marotzke, J., Matei, D., Mikolajewicz, U., Notz, D., and Storch, J. S.: Characteristics of the ocean simulations in MPIOM, the ocean component of the MPI-Earth system model, J. Adv. Model.
510 Earth Syst., 5(2), 422–446, doi:10.1002/jame.20023, 2013.

16

Kalnay, E., Kanamitsu, M., Kistler, R., Collins, W., Deaven, D., Gandin, L., Iredell, M., Saha, S., White, G., Woollen, J., Zhu, Y., Chelliah, M., Ebisuzaki, W., Higgins, W., Janowiak, J., Mo, K. C., Ropelewski, C., Wang, J., Leetmaa, A., Reynolds, R., Jenne, R., and Joseph, D.: The NCEP/NCAR 40-year reanalysis project, Bull. Amer. Meteor. Soc., 77(3), 437–471, doi:10.1175/1520-0477(1996)077<0437:TNYRP>2.0.CO;2, 1996.

515 Kaplan, A., Cane, M., Kushnir, Y., Clement, A., Blumenthal, M., and Rajagopalan, B.: Analyses of global sea surface temperature 1856-1991, J. Geophys. Res., 103 (C9), 18567-18589, doi:10.1029/97JC01736, 1998.

Kida, S., Price, J. F., and Yang, J.: The upper-oceanic response to overflows: A mechanism for the Azores Current, J. Phys. Oceanogr., 38(4), 880–895, doi:10.1175/2007JPO3750.1, 2008.

Kida, S., Richards, K. J., and Sasaki, H.: The fate of surface freshwater entering the Indonesian Seas, J. Geophys. Res.: Oceans, 520 124(5), 3228–3245, doi: 10.1029/2018JC014707, 2019.

~~Kwok, R., Cunningham, G. F., and Pang, S. S.: Fram Strait sea-ice outflow, J. Geophys. Res., 109 (C1), C01009, doi:10.1029/2003JC001785, 2004.~~

Kobayashi, S., Ota, Y., Harada, Y., Ebita, A., Moriya, M., Onoda, H., Onogi, K., Kamahori, H., Kobayashi, C., Endo, H., Miyaoka, K., and Takahashi, K.: The JRA-55 reanalysis: General specifications and basic characteristics. J. Meteorol. Soc. 525 of JPN Ser. II, 93(1), 5–48, doi:10.2151/jmsj.2015-001, 2015.

Koch-Larrouy, A., Madec, G., Bouruet-Aubertot, P., Gerkema, T., Bessières, L., and Molcard, R.: On the transformation of Pacific Water into Indonesian Throughflow Water by internal tidal mixing, Geophys. Res. Lett., 34, L04604, doi:10.1029/2006GL028405, 2007.

Komori, N., Takahashi, K., Komine, K., Motoi, T., Zhang, X., and Sagawa, G.: Description of sea-ice component of coupled 530 ocean sea-ice model for the earth simulator (OIFES), J. Earth Simulator, 4, 31–45, https://www.jamstec.go.jp/ceist/j/publication/journal/jes_vol.4/pdf/JES4_24_komori.pdf, 2005.

Kurogi, M., Tanaka, Y., and Hasumi, H.: Effects of deep bottom topography on the Kuroshio Extension studied by a nested-grid OGCM, CLVAR Exchanges, 69 (20), 19–21, http://www.clivar.org/sites/default/files/documents/Exchanges_69.pdf, 2016.

535 Kutsuwada, K.: Impact of wind/wind-stress field in the North Pacific constructed by ADEOS/NSCAT data, J. Oceanogr., 54(5), 443–456, doi:10.1007/BF02742447, 1998.

Kutsuwada, K., Kakiuchi, A., Sasai, Y., and Sasaki, H.: Wind-driven North Pacific Tropical Gyre using high-resolution simulation outputs, J. Oceanogr., 75 (1), 81–93, doi:10.1007/s10872-018-0487-8, 2019.

Kwok, R., Cunningham, G. F., and Pang, S. S.: Fram Strait sea ice outflow, J. Geophys. Res., 109 (C1), C01009, 540 doi:10.1029/2003JC001785, 2004.

Large W., and Yeager S.: Diurnal to decadal global forcing for ocean and sea-ice models: The data sets and flux climatologies, NCAR Technical Note NCAR/TN-460+STR, doi:10.5065/D6KK98Q6, 2004.

Large, W. G., McWilliams, J. C., and Doney, S. C.: Oceanic vertical mixing: A review and a model with a nonlocal boundary layer parameterization, Rev. Geophys., 32(4), 363– 403, doi:10.1029/94RG01872, 1994.

17

545 Lindzen, R. S. and Nigam, S.: On the role of sea surface temperature gradients in forcing low-level winds and convergence in the tropics, J. Atmos. Sci., 44(17), 2418–2436, doi:10.1175/1520-0469(1987)044<2418:OTROSS>2.0.CO;2, 1987.

Locarnini, R. A., Mishonov, A. V., Antonov, J. I., Boyer, T. P., Garcia, H. E., Baranova, O. K., Zweng, M. M., Paver, C. R., Reagan, J. R., Johnson, D. R., Hamilton, M., and Seidov, D.: World Ocean Atlas 2013, Volume 1: Temperature. S. Levitus, Ed., A. Mishonov Technical Ed.; NOAA Atlas NESDIS 73, 40 pp, doi:10.7289/V55X26VD, 2013.

550 ~~McWilliams, J.C., Gula, J., and Molemaker, M.J.: The Gulf Stream North wall: Ageostrophic circulation and frontogenesis, J. Phys. Oceanogr., 49, 893–916, https://doi.org/10.1175/JPO-D-18-0203.1, 2019.~~

Maltrud, M. E. and McClean, J. L.: An eddy resolving global 1/10° ocean simulation, Ocean Modelling, 8 (1–2), 31–54, doi:10.1016/j.ocemod.2003.12.001, 2005.

Masumoto, Y.: Sharing the results of a high-resolution ocean general circulation model under a multi-discipline framework—
555 a review of OFES activities, Ocean Dyn., 60 (3), 633–652, doi:10.1007/s10236-010-0297-z, 2010.

Masumoto, Y., Sasaki, H., Kagimoto, T., Komori, N., Ishida, A., Sasai, Y., Miyama, T., Motoi, T., Mitsudera, H., Takahashi, k., Sakuma, H., and Yamagata, T.: A fifty-year eddy-resolving simulation of the world ocean—Preliminary outcomes of OFES (OGCM for the Earth Simulator), J. Earth Simulator, 1, 35–56, doi:10.32131/jes.1.35, 2004.

Masumoto, Y., Morioka, Y., and Sasaki, H.: High-resolution Indian Ocean simulations – Recent advances and issues from
560 OFES-.In Ocean Modeling in an Eddying Regime, edited by: Hecht, M. W., Hasumi, H., Geophysical Monograph Series, 177, AGU, Washington D.C., 165–175. doi:10.1029/177GM14, 2008.

McCartney, M.S. and Mauritzen, C.: On the origin of the warm inflow to the Nordic Seas, Prog. Oceanogr. 51 (1), 125–214, doi:10.1016/S0079-6611(01)00084-2, 2001.

McWilliams, J.C., Gula, J., and Molemaker, M.J.: The Gulf Stream North wall: Ageostrophic circulation and frontogenesis, J.
565 Phys. Oceanogr., 49, 893–916, https://doi.org/10.1175/JPO-D-18-0203.1, 2019.

Nagai, T., Hibiya, T., and Bouruet-Aubertot, P.: Nonhydrostatic simulations of tide-induced mixing in the Halmahera Sea: A possible role in the trans formation of the Indonesian Throughflow waters, J. Geophys. Res.: Oceans, 122, 8933–8943, doi:10.1002/2017JC013381, 2017.

Nakamura, T., Toyoda, T., Ishikawa, Y., and Awaji, T.: Enhanced ventilation in the Okhotsk Sea through tidal mixing at the
570 Kuril Straits, Deep Sea Res. PT I: Oceanogr. Res. Pap., 53 (3), 425–448, doi:10.1016/j.dsr.2005.12.006, 2006.

Nakano, T., Kitamura, T., Sugimoto, S., Suga, T., and Kamachi, M.: Long-term variations of North Pacific Tropical Water along the 137°E repeat hydrographic section, J. Oceanogr., 71 (3), 229–238, doi:10.1007/s10872-015-0279-3, 2005.

Noh, Y. and Kim, H. J.: Simulations of temperature and turbulence structure of the oceanic boundary layer with the improved near-surface process, J. Geophys. Res., 104 (C7), 15621–15634, doi:10.1029/1999JC900068, 1999.

575 Nonaka, M., Sasai, Y., Sasaki, H., Taguchi, B., and Nakamura, H.: How potentially predictable are midlatitude ocean currents?, Scientific Reports, 6, 20153. doi:10.1038/srep20153, 2016.

Pacanowski, R. C. and Griffies, S. M.: The MOM3 manual. GFDL Ocean Group Tech. Rep. 4, NOAA. Geophysical Fluid Dynamics Laboratory, Princeton, NJ., https://www.gfdl.noaa.gov/wp-content/uploads/files/model_development/ocean/mom3_manual.pdf, 1999.

580 Prasad, T. G., Ikeda, M., and Kumar, S.P.: Seasonal spreading of the Persian Gulf Water mass in the Arabian Sea, J. Geophys. Res.: Oceans, 106 (C8), 17059–17071, doi:10.1029/2000JC000480, 2001.

Qiu, B. and Chen, S.: Eddy-mean flow interaction in the decadally-modulating Kuroshio Extension system, Deep Sea Res. PT II: Trop. Stud. Oceanogr., 57, 1098–1110, doi:10.1016/j.dsr2.2008.11.036, 2010.

Qiu, B., Chen, S., Klein, P., Wang, J., Torres, H., Fu, L., and Menemenlis, D.: Seasonality in transition scale from balanced to
585 unbalanced motions in the world ocean, J. Phys. Oceanogr., 48 (3), 591–605, doi:10.1175/JPO-D-17-0169.1, 2018.

Rayner, N. A., Parker, D. E., Horton, E. B., Folland, C. K., Alexander, L. V., Rowell, D. P., Kent, E. C., and Kaplan, A. (2003). Global analyses of sea surface temperature, sea ice, and night marine air temperature since the late nineteenth century, J. Geophys. Res.: Atmos., 108 (D14), 4407, doi:10.1029/2002JD002670, 2003.

Reid, J.L.: On the contribution of the Mediterranean Sea outflow to the Norwegian-Greenland Sea, Deep Sea Res. A.
590 Oceanogra. Res. Pap., 26 (11), 1199–1223, doi:10.1016/0198-0149(79)90064-5, 1979.

Renault, L., McWilliams, J.C., and Penven, P.: Modulation of the Agulhas current retroflection and leakage by oceanic current interaction with the atmosphere in coupled Simulations. J. Phys. Oceanogr., 47 (8), 2077–2100, doi:10.1175/JPO-D-16-0168.1, 2017.

Renault, L., Marchesiello, P., Masson, S., and McWilliams, J. C.: Remarkable control of western boundary currents by eddy
595 killing, a mechanical air-sea coupling process, Geophys. Res. Lett., 46 (5), 2743–2751, doi:10.1029/2018GL081211, 2019a.

Renault, L., Masson, S., Oerder, V., Jullien, S., and Colas, F.: Disentangling the mesoscale ocean-atmosphere interactions. J. Geophys. Res. Oceans, 124 (3) , 2164–2178, doi:10.1029/2018JC014628, 2019b.

Renault, L., Masson, S., Arsouze, T., Madec, G., and McWilliams, J. C.: Recipes for how to force oceanic model dynamics, J. Adv. Mod. Ear. Sys., 12 (2), e2019MS001715, doi:10.1029/2019MS001715, 2020.

600 Reynolds, R. W.: A real-time global sea surface temperature analysis, J. Clim., 1 (1), 75–86, doi:10.1175/1520-0442(1988)001<0075:ARTGSS>2.0.CO;2, 1988.

Roemmich, D., Johnson, G., Riser, S., Davis, R., Gilson, J., Owens, W. B., Garzoli, S. L., Schmid, C., and Ignaszewski, M. (2009). The Argo program: Observing the global ocean with profiling floats. Oceanography, 22 (2), 34–43, doi: 10.5670/oceanog.2009.36, 2009.

605 Rosati, A. and Miyakoda, K.: A general circulation model for upper ocean circulation, J. Phys. Oceanogr., 18 (11), 1601–1626, doi:10.1175/1520-0485(1988)018<1601:AGCMFU>2.0.CO;2, 1988.

Saji, N. H., Goswami, B. N., Vinayachandran, P. N., and Yamagata, T.: A dipole mode in the tropical Indian Ocean, Nature, 401 (6751), 360, doi:10.1038/43854, 1999.

19

Sasaki, H., Sasai, Y., Nonaka, M., Masumoto, Y., and Kawahara, S.: An eddy-resolving simulation of the quasi-global ocean
610   driven by satellite-observed wind field: Preliminary outcomes from physical and biological fields, J. Earth Simulator, 6,
          35–49, https://www.jamstec.go.jp/ceist/j/publication/journal/jes_vol.6/pdf/JES6_24-Sasaki.pdf, 2006.

Sasaki, H., Nonaka, M., Masumoto, Y., Sasai, Y., Uehara, H., and Sakuma, H.: An eddy-resolving hindcast simulation of the
          quasiglobal ocean from 1950 to 2003 on the Earth Simulator, edited by Hamilton, K., Ohfuchi, W., High Resolution
          Numerical Modelling of the Atmosphere and Ocean, Springer, New York, NY, 157–186. https://doi.org/10.1007/978-0-
615   387-49791-4_10, 2008.

Sasaki, H., Klein, P., Qiu, B., and Sasai, Y. (2014).: Impact of oceanic scale-interactions on the seasonal modulation of ocean
          dynamics by the atmosphere. Nature Communications, 5, 5636, doi:10.1038/ncomms6636, 2014.

Sasaki, H., Kida, S., Furue, R., Nonaka, M., and Masumoto, Y.: An increase of the Indonesian Throughflow by internal tidal
          mixing in a high-resolution quasi-global ocean simulation, Geophys. Res. Lett., 45 (16), 8416–8424,
620   doi:10.1029/2018GL078040, 2018.

Sasaki, Y. N. and Schneider, N.: Decadal shifts of the Kuroshio Extension jet: application of thin–jet theory, J. Phys. Oceanogr.,
          41, 979–993, doi:10.1175/2011JPO4550.1, 2011.

Schoonover, J., Dewar, W., Wienders, N., Gula, J., McWilliams, J.C., Molemaker, M.J., Bates, S.C., Danabasoglu, G.and
          Yeager, S.: North Atlantic barotropic vorticity balances in numerical models, J. Phys. Oceanogr., 46 (1), 289–303,
625   doi:10.1175/JPO-D-15-0133.1, 2016.

Schoonover, J., Dewar, W., Wienders, and Deremble, B.: Local sensitivities of the Gulf Stream separation, J. Phys. Oceanogr.,
          47 (2), 353–373, doi:10.1175/JPO-D-16-0195.1, 2017.

Sofianos, S. S. and Johns, W. E.: An Oceanic General Circulation Model (OGCM) investigation of the Red Sea circulation, 1,
          Exchange between the Red Sea and the Indian Ocean, J. Geophys. Res.: Oceans, 107 (C11), 3196,
630   doi:10.1029/2001JC001184, 2002.

St. Laurent, L. C., Simmons, H. L., and Jayne, S. R.: Estimating tidally driven mixing in the deep ocean, Geophys. Res. Lett.,
          29 (23), 2106, doi:10.1029/2002GL015633, 2002.

Taguchi, B., Schneider, N., Nonaka, M, and Sasaki, H.: Decadal variability of upper-ocean heat content associated with
          meridional shifts of western boundary current extensions in the North Pacific, J. Clim., 30, 6247–6264, doi:10.1175/JCLI-
635   D-16-0779.1, 2017.

Tanaka, Y., Hibiya, T., and Niwa, Y.: Estimates of tidal energy dissipation and diapycnal diffusivity in the Kuril Straits using
          TOPEX/POSEIDON altimeter data, J. Geophys. Res.: Oceans, 112 (C10), C10021, doi:10.1029/2007JC004172, 2007.

Tanaka, Y., Hibiya, T., and Niwa, Y.: Assessment of the effects of tidal mixing in the Kuril Straits on the formation of the
          North Pacific Intermediate Water, J. Phys. Oceanogr., 40 (12), 2569–2574, doi:10.1175/2010JPO4506.1, 2010.

640   Tsujino, H., Nishikawa, S., Sakamoto, K., Usui, N., Nakano, H., and Yamanaka, G.: Effects of large-scale wind on the
          Kuroshio path south of Japan in a 60-year historical OGCM simulation, Clim. Dyn., 41, 2287–2318, doi:10.1007/s00382-
          012-1641-4, 2013.

Tsujino, H., Urakawa, S., Nakano, H., Small, R. J., Kim, W. M., Yeager, S. G., Danabasoglu, G., Suzuki, T., Bamber, J. L., Bentsen, M., Böning, C. W., Bozec, A., Chassignet, E. P., Curchitser, E., Dias, F. B., Durack, P. J., Griffies, S. M., Harada, Y., Ilicak, M., Josey, S. A., Kobayashi, C., Kobayashi, S., Komuro, Y., Large, W. G., Le Sommer, J., Marsland, S. J., Masina, S., Scheinert, M., Tomita, H., Valdivieso, M., Yamazaki, D.: JRA-55 based surface dataset for driving ocean–sea-ice models (JRA55-do), Ocean Modell., 130, 79–139, doi:10.1016/j.ocemod.2018.07.002, 2018.

Wallace, J. M., Michell, T. P., and Deser, C.: The influence of sea-surface temperature on surface wind in the eastern equatorial Pacific: Seasonal and interannual variability, J. Clim., 2 (12), 1492–1499, doi:10.1175/1520-0442(1989)002<1492:TIOSST>2.0.CO;2, 1989.

Wentz, F. J. and Meissner, T.: Supplement 1: Algorithm theoretical basis document for AMSR-E ocean algorithms, Remote Sensing Systems Tech. Rep. 051707, 6 pp, http://images.remss.com/papers/rsstech/2007_051707_Wentz_AMSR_Ocean_V2_Supplement_1.pdf, 2007.

Zhai, X. and Greatbatch, R. J.: Wind work in a model of the northwest Atlantic Ocean, Geophys. Res. Lett., 34 (4), L04606, doi:10.1029/2006GL028907, 2007.

Zhai, X., Greatbatch, R. J., and Kohlmann, J. D.: On the seasonal variability of eddy kinetic energy in the Gulf Stream region, Geophys. Res. Lett., 35, L24609, doi:10.1029/2008GL036412, 2008.

Zweng, M. M., Reagan, J. R., Antonov, J. I., Locarnini, R. A., Mishonov, A. V., Boyer, T. P., Garcia, H. E., Baranova, O. K., Johnson, D. R., Seidov, D., and Biddle, M. M.: World Ocean Atlas 2013, Volume 2: Salinity. S. Levitus, Ed., A. Mishonov Technical Ed.; NOAA Atlas NESDIS 74, 39 pp, doi:10.7289/V5251G4D, 2013.
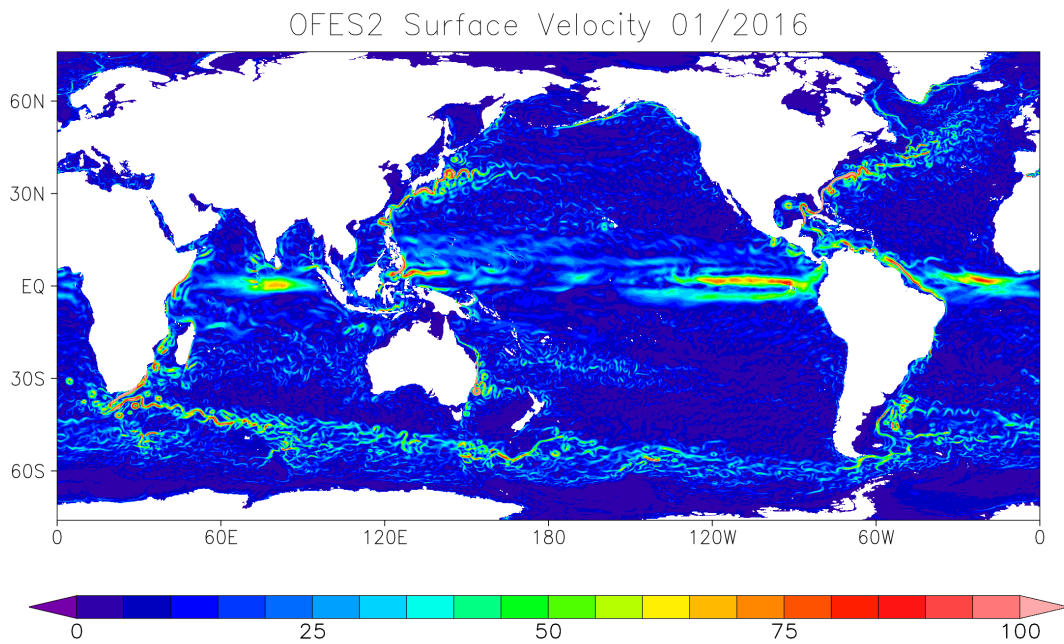
Figure 1: An example of monthly averaged surface current speeds (cm s⁻¹) in OFES2.
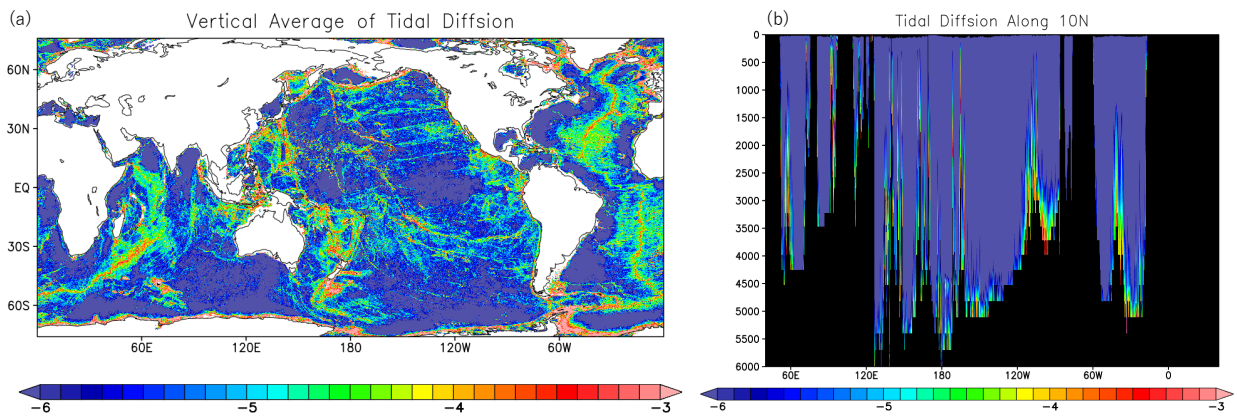
Figure 2: Daily mean vertical diffusivity (log10 m² s⁻¹) on December 1, 2016 estimated by the tidal mixing scheme (a) vertically averaged from the surface to the bottom and (b) in the vertical section along 10° N.
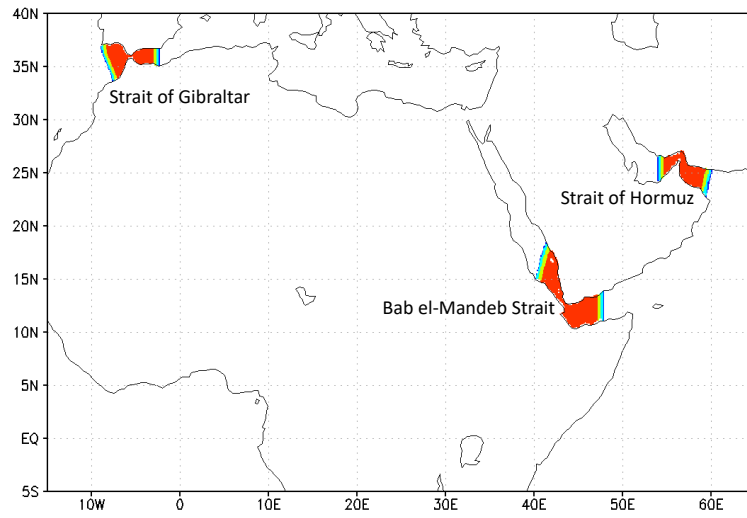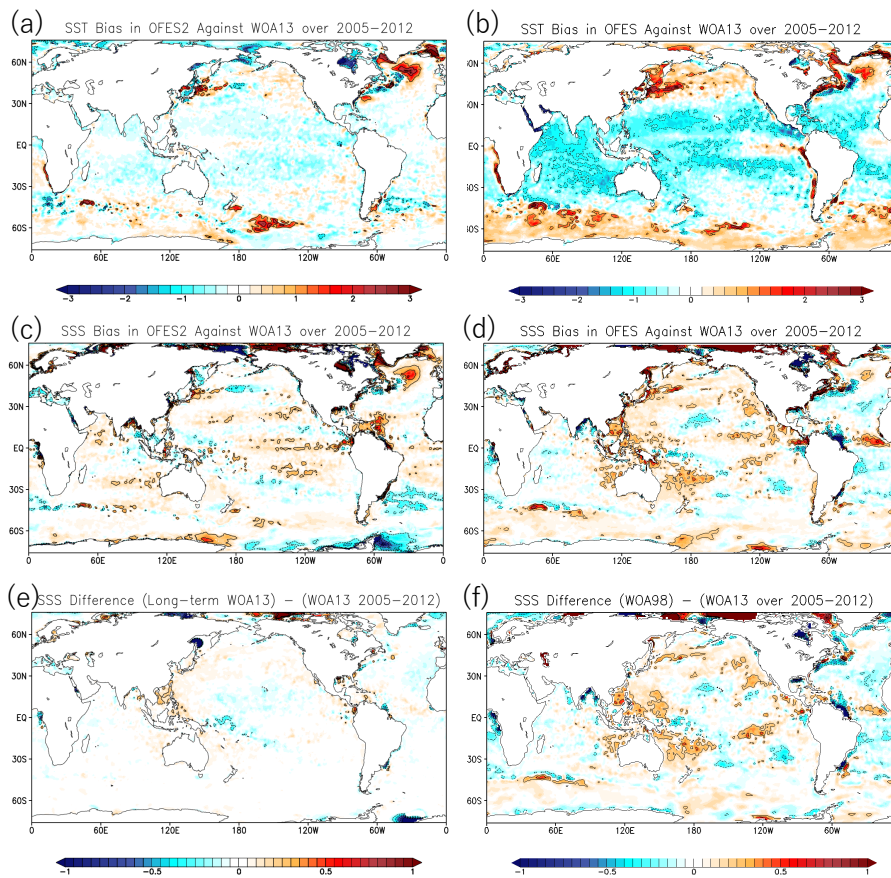
22

Figure 3: Timescales for restoring the temperature and salinity in and near the Straits of Gibraltar, Hormuz, and Bab el-Mandeb. Red, yellow, light blue, and blue represent timescales of 1, 5, 10, and 30 days, respectively.

675 **Figure 4: SST bias (°C) in (a) OFES2 and (b) OFES averaged over 2005-2012 against WOA13. (c) and (d) are the same as in (a) and (b), respectively, but the SSS bias is shown instead (psu). SSS differences in (e) long-term WOA13 and (f) WOA98 from WOA13 averaged over 2005-2012. The contour lines are superimposed at an interval of 1 °C for SST and 0.2 psu for SSS, but zero contour lines are omitted.**
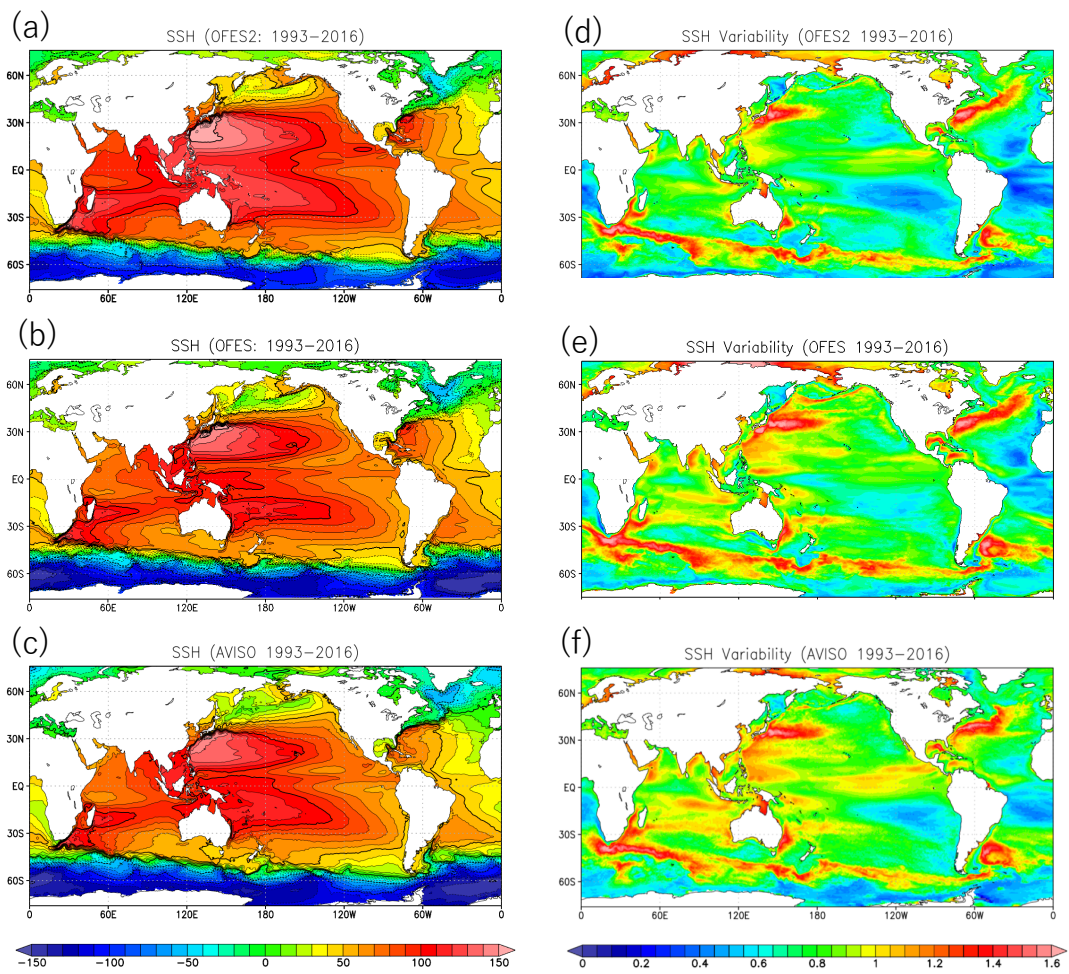
680 **Figure 5: Mean (a, b, c) SSH (cm) and (d, e, f) its standard deviation (log10 cm) averaged over 1993-2016 from (a, d) OFES2, (b, e) OFES, and (c, f) AVISO observations. The SSH in OFES2 and OFES was offset by adding 50 cm.**
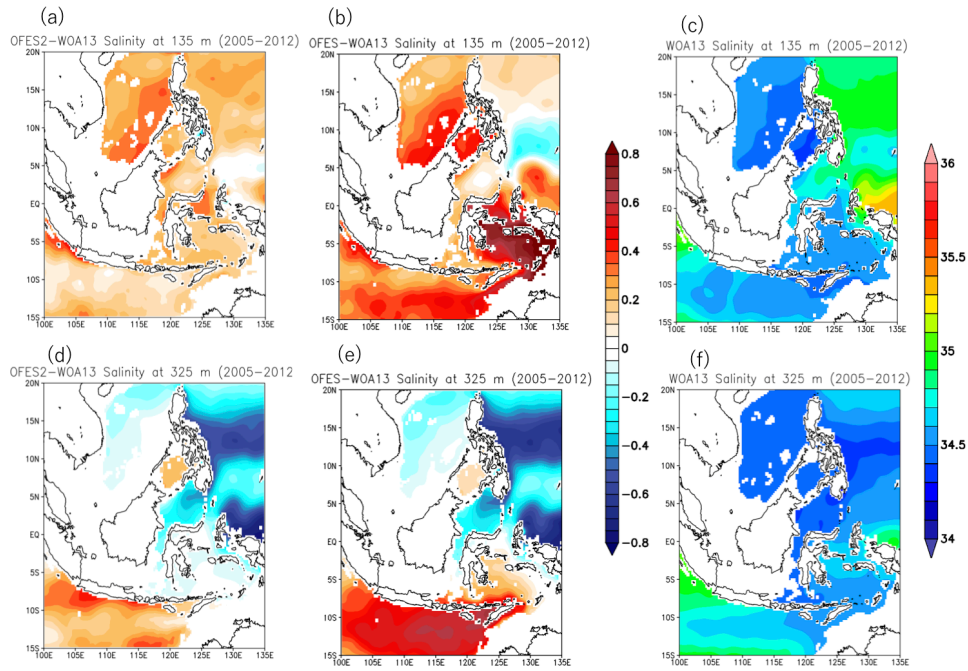
Figure 6: Salinity biases (a, b, d, e) against WOA13 (c, f) in OFES2 (a, d), OFES (b, e) at 135 m (a, b, c) and at 325 m (d, e, f). All fields are averaged over 2005-2012, and the units are psu.
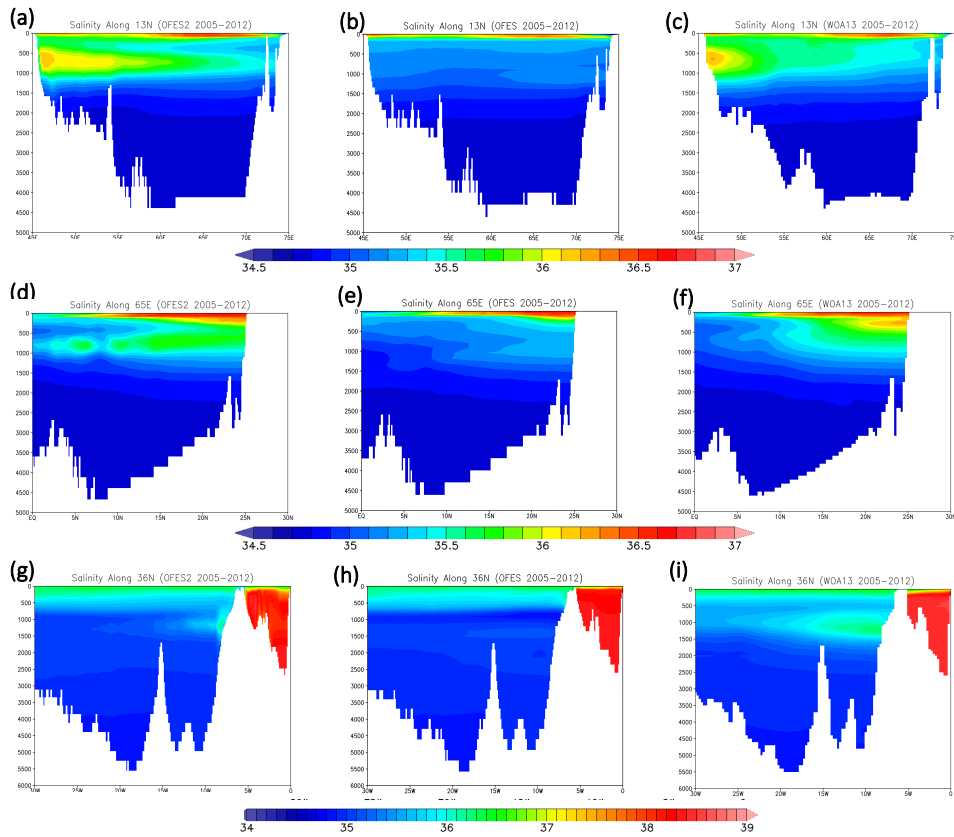
685

Figure 7: Vertical sections of mean salinity along (a-c) 13° N and (d-f) 65° E in the Arabian Sea and (g-i) 36° N in the eastern Atlantic Ocean averaged over 2005-2012: (a, d, g) OFES2, (b, e, h) OFES, and (c, f, i) WOA13.
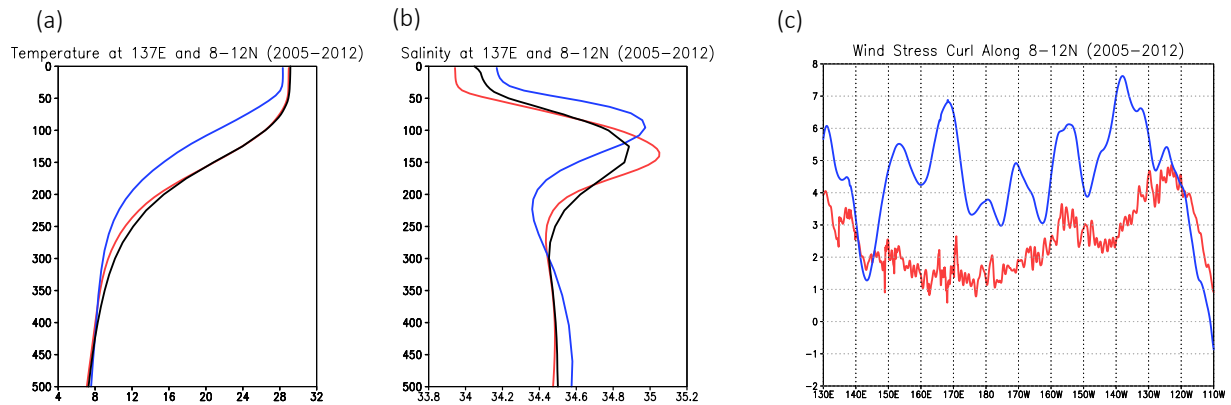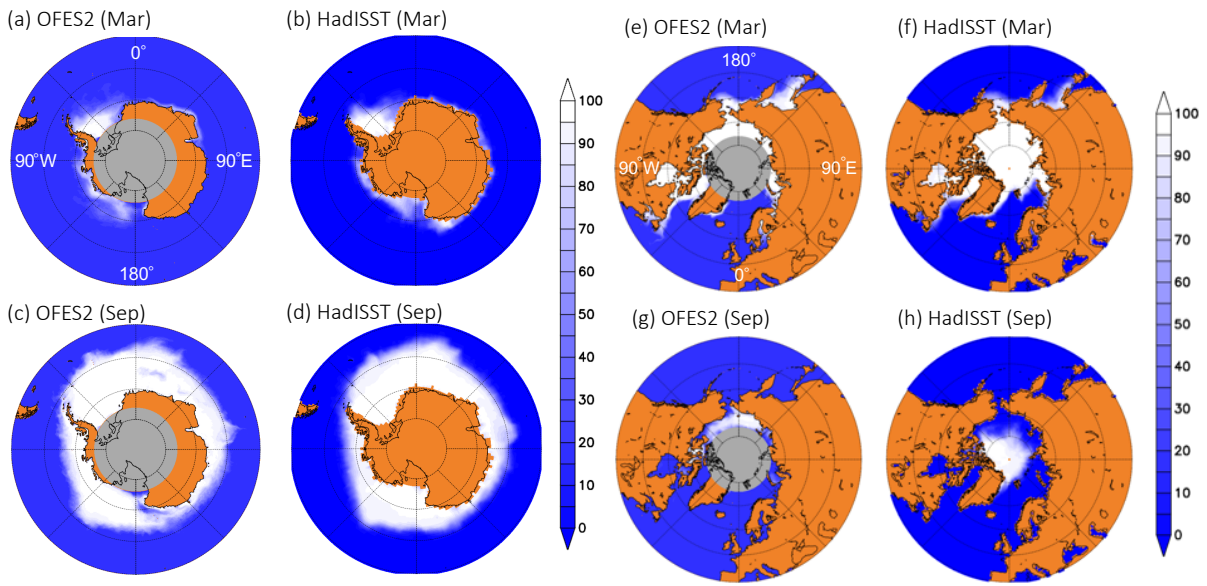

Figure 8: Vertical profile of (a) temperature (°C) and (b) salinity (psu) at 137°E averaged from 8°N to 12°N and over 2005–2012. (c)
690 **Longitudinal distributions of the wind stress curl (10^{-8} N m^{-3}) along 10° N (averaged from 8° N to 12° N and over 2005-2012). The red, blue, and black curves are OFES2 driven by JRA55-do, OFES driven by NCEP reanalysis, and the WOA13 observations, respectively.**

27

Figure 9: Sea-ice concentrations (%) in the Antarctic Ocean in (a, b) March and (c, d) September in (a, c) OFES2 and (b, d) HadISST averaged over 2005-2012. Similarly, the sea-ice concentrations in Arctic Ocean in (e, f) March and (g, h) September in (e, g) OFES2 and (f, h) HadISST. The gray areas are out of the model domain in OFES2 (a, c, e, g).
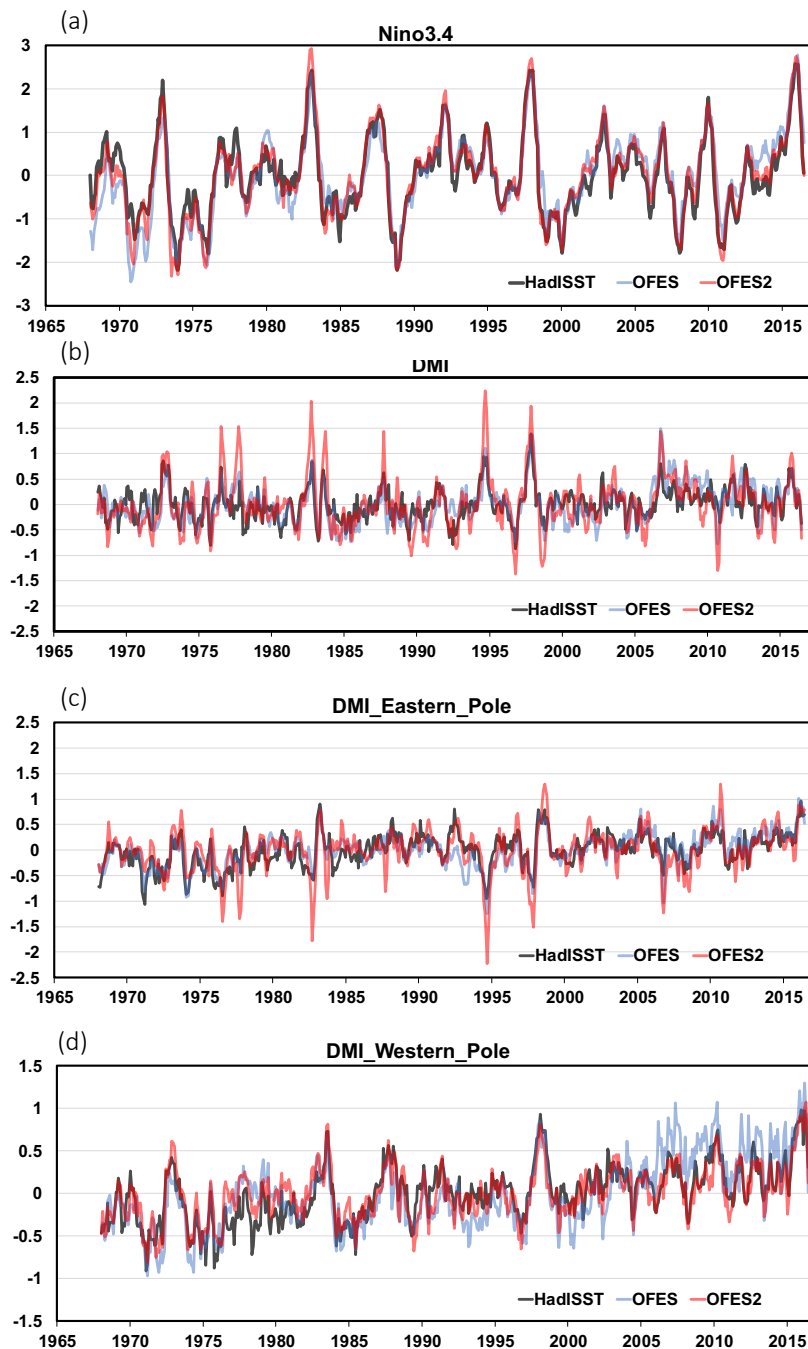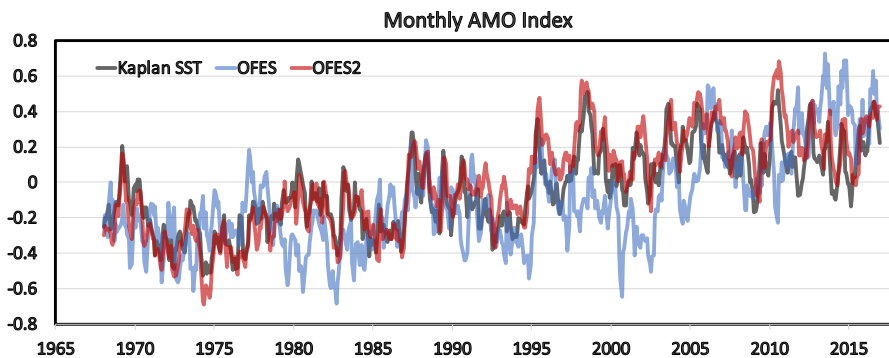
Figure 10: (a) Monthly Niño3.4 index defined as SSTAs (°C) in 165°-145° W and 5° S-5° N in the eastern topical Pacific and (b) the monthly DMI (°C) defined as difference between the SSTAs (°C) in the (c) eastern (90° E-110° E, 10° S-0°) and (d) the western (50°-70° E and 10° S-10° N) poles (Saji et al. 1999) from OFES2 (red curve), OFES (blue curve), and HadISST version 1 (black curve, http://www.cpc.ncep.noaa.gov/data/indices/ and http://www.jamstec.go.jp/frcgc/research/d1/iod/iod/dipole_mode_index.html).

29
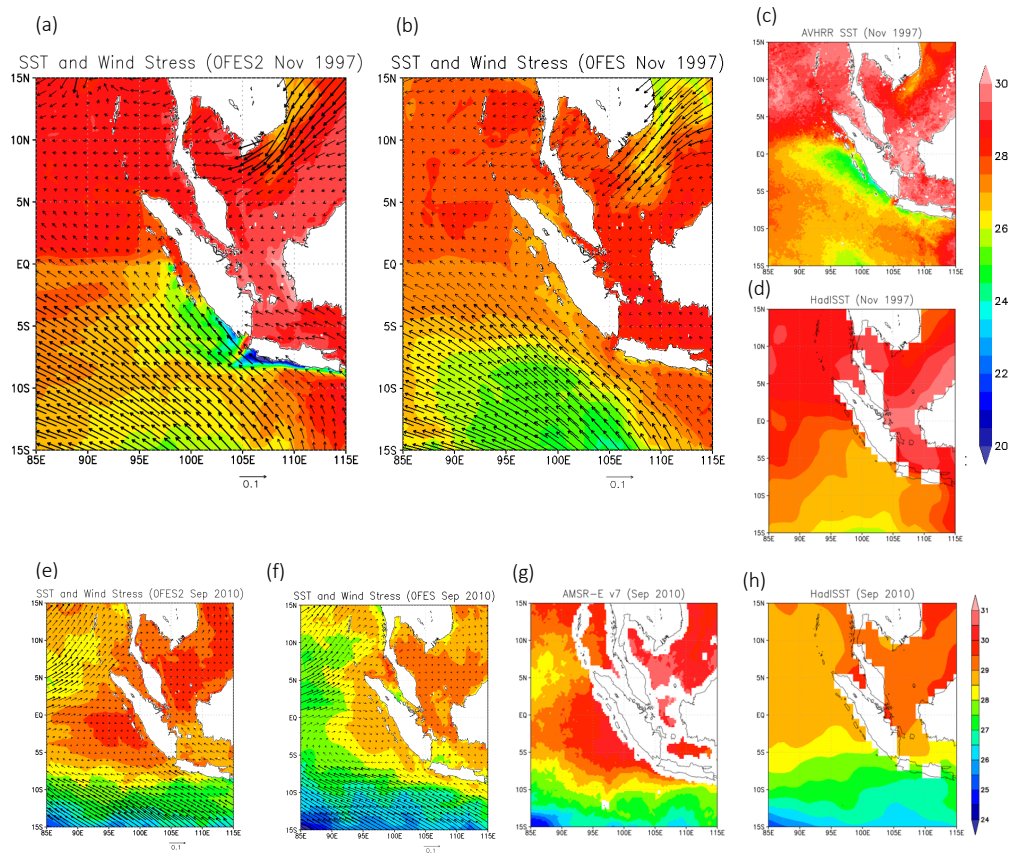
Figure 11: SST (°C) in a region including the IOD eastern pole (90°-110° E and 10° S-0°) in the mature month of (a-d) the 1997 positive IOD event (November 1997) and (e-h) the 2010 negative IOD event (September 2010). (a, e) OFES2, (b, f) OFES, (c, g) satellite observations of AVHRR version 4.1 (Casey et al. 2010) and AMSR-E version 7 (Wentz & Meissner 2007), and (d, h) HadISST ver.1 (Rayner et al. 2003). The vectors in (a, b, e, f) are the surface wind stress (N m⁻²) in the models, which are plotted at a 1°×1° resolution. The thick vectors denote wind stress magnitudes stronger than 0.05 N m⁻².

Figure 12: Monthly AMO index defined as SSTAs (°C) in 0° S-70° N in the eastern topical Pacific in the Kaplan SST (black curve, Kaplan et al. 1998, https://psl.noaa.gov/data/timeseries/AMO/), OFES2 (red curve), and OFES (blue curve).

	OFES2	OFES
Domain	76°S-76°N	75°S-75°N
Horizontal Resolution	0.1°	0.1°
Number of Vertical Levels	105	54
Maximum Depth	7,500 m	6,065 m
Bathymetry Data	ETOPO1	OCCAM 30'
Sea-Ice Model	Komori et al. 2005	-
Horizontal Mixing Scheme	Biharmonic	Biharmonic
Vertical Mixing Scheme	Noh & Kim 1999	KPP (Large et al. 1994)
Tidal Mixing Scheme	St. Laurent et al. 2002	-
SSS Restoring	15 days to WOA13	6 days to WOA98
Northern/Southern Artifical Boundary	T & S restoring within 3° from the boundary	T & S restoring within 3° from the boundary
Important Narrow Channels	Straits of Gibraltar, Hormuz, and Bab el-Mandeb	-
Atmospheric Forcing	JRA55-do (3 hourly, 55km x 55km)	NCEP (daily, 2.5° x 2.5°)
River Runoff	CORE2 (monthly climatology)	-
Bulk Formula	Large & Yeager 2004	Rosati & Miyakoda 1988
Momentum Flux	Bulk formula using the relative wind speed	Momentum flux in NCEP (daily)
Hindcast Period	1958-2016	1950-2017
Initial Condition	T & S of OFES on Jan 1, 1958	OFES climatlogical run
Outputs	Daily mean every 3 days until 1989 Daily mean from 1990 Monthly mean	Snapshot every 3 days from 1980 Monthly Mean

Table 1: Descriptions of the quasi-global eddying hindcast simulations of OFES2 and OFES.

31

(a)

	OFES2	OFES	HadISST
RMS Amplitude of the Niño 3.4 index（℃）	0.95	0.93	0.89
Correlation with the Niño 3.4 in HadISST	0.963	0.880	-
RMS Amplitude of the DMI（℃）	0.52	0.38	0.32
Correlation with the DMI in HadISST	0.714	0.659	-

(b)

	OFES2	OFES	HadISST
RMS Amplitude of the Eastern Pole DMI(℃)	0.43	0.33	0.33
Correlation with the Eastern Pole DMI in HadISST	0.713	0.749	-
RMS Amplitude of the Western Pole DMI（℃）	0.31	0.41	0.33
Correlation with the Western Pole DMI in HadISST	0.847	0.751	-

Table 2: (a) RMS amplitude (°C) of the Niño3.4 index and the DMI for OFES2, OFES, and HadISST and their correlations between OFES2 and HadISST and between OFES and HadISST. (b) Same as (a) but the eastern and western pole DMIs.

	Improvements in OFES2 over OFES	New or remaining issues in OFES2
SST (3.1.1)	Suppressed cold biases in the equatorial and subtropical regions Suppressed warm biases in the high-latitude regions, the Arctic Ocean, the Sea of Okhotsk, and along the west coasts of South America and South Africa	Warm biases in the South Pacific and to the north of the Kuroshio Extension Warm and cold biases along the Gulf Stream
SSS (3.1.1)	Suppressed large biases by relatively weak SSS restoring	Salty biases in the North Atlantic and northern part of the Bay of Bengal and to the north of the South America
Mean SSH (3.1.2)	More realistic gyres in the subtropical North and South Pacific Suppressed too distinct propagations of the Agulhas Rings	Unrealistic pathways of the Gulf Stream and Kuroshio No Azores Current
SSH variability (3.1.2)	Suppressed too large variability along the strong currents	Slightly small in the regions away from the strong currents
Water property (3.2, 3.3, 3.4)	Suppressed biases in the subsurfaces of the Indonesian Seas, the Arabian Sea (salty outflows from the Persian Gulf and Red Sea), and the subtropical western Pacific	Lack of nonlocal tidal mixing in the Indonesian Seas Unrealistic subsurface in the northeastern subtropical Atlantic Ocean (salty outflow from the Mediterranean Sea)
El Niño and IOD (4)	Slightly higher correlations of the indexes with observations More realistic SST near the Sumatra and Java during the IOD events	

Table 3: Improvements in OFES2 over OFES and new or remaining issues in OFES2.

32